Preserving the Boltzmann ensemble in replica-exchange molecular dynamics

Ben Cooke[1] and Scott C. Schmidler[2,a)]
[1]*Department of Mathematics, Duke University, Durham, North Carolina 27708-0251, USA*
[2]*Department of Statistical Science, Program in Computational Biology and Bioinformatics, and Program in Structural Biology and Biophysics, Duke University, Durham, North Carolina 27708-0251, USA*

(Received 16 April 2008; accepted 5 September 2008; published online 27 October 2008)

We consider the convergence behavior of replica-exchange molecular dynamics (REMD) [Sugita and Okamoto, Chem. Phys. Lett. **314**, 141 (1999)] based on properties of the numerical integrators in the underlying isothermal molecular dynamics (MD) simulations. We show that a variety of deterministic algorithms favored by molecular dynamics practitioners for constant-temperature simulation of biomolecules fail either to be measure invariant or irreducible, and are therefore not ergodic. We then show that REMD using these algorithms also fails to be ergodic. As a result, the entire configuration space may not be explored even in an infinitely long simulation, and the simulation may not converge to the desired equilibrium Boltzmann ensemble. Moreover, our analysis shows that for initial configurations with unfavorable energy, it may be impossible for the system to reach a region surrounding the minimum energy configuration. We demonstrate these failures of REMD algorithms for three small systems: a Gaussian distribution (simple harmonic oscillator dynamics), a bimodal mixture of Gaussians distribution, and the alanine dipeptide. Examination of the resulting phase plots and equilibrium configuration densities indicates significant errors in the ensemble generated by REMD simulation. We describe a simple modification to address these failures based on a stochastic hybrid Monte Carlo correction, and prove that this is ergodic. © *2008 American Institute of Physics*. [DOI: 10.1063/1.2989802]

I. INTRODUCTION

The replica-exchange molecular dynamics (REMD) algorithm[1] has become a widely used tool for molecular simulation. The REMD algorithm is an adaptation to molecular dynamics (MD) of the Metropolis-coupled Markov chain Monte Carlo (or *parallel tempering*) algorithm,[2] which enables the crossing of large energy barriers through swapping of parallel simulations at a ladder of increasing temperatures. The REMD algorithm has recently seen wide popularity for simulations of complex molecules such as peptides and proteins[3–9] due to empirical evidence that simulations equilibrate dramatically faster. Indeed, recent theoretical results for parallel tempering Monte Carlo show that a range of sampling problems converge exponentially faster when parallel tempering is applied compared with standard Metropolis algorithms,[10,11] although such speedups do not necessarily occur for every system.[12,13]

Although REMD was derived from parallel tempering, a Monte Carlo algorithm which has certain desirable characteristics, REMD does not necessarily inherit these characteristics. Chief among these is the ability to generate configurations according to the Boltzmann ensemble, a key condition for computing experimental observables from simulation. In this paper we consider convergence behavior of the REMD algorithm as commonly implemented in biomolecular simulation, focusing on certain theoretical shortcomings and their practical implications. In particular, we emphasize the properties of measure invariance and ergodicity, show that the isothermal dynamics algorithms commonly used for REMD do not exhibit these properties, and that as a result REMD using these standard integrators also fails to exhibit these properties.

After a brief statement of the REMD algorithm, we review necessary and sufficient conditions for dynamical systems and their integrators to be measure-preserving and ergodic. We then examine several commonly used and proposed techniques for the isothermal dynamics required by REMD and show that all fail to satisfy these conditions. By proving rigorously these failures, we resolve ambiguity in the literature stemming from purely empirical studies and assumptions. We also show that combining these dynamics via replica exchange does not correct this problem. In some cases these failures of the underlying constant-temperature algorithms are known, while in others our results are new; however, in all cases the impact on the theoretical properties and practical performance of REMD does not appear to have been appreciated. We conclude by showing that these failures can be addressed by the addition of stochastic hybrid Monte Carlo corrections, and demonstrate the significant practical ditferences obtained on some simple Hamiltonian systems.

II. REPLICA-EXCHANGE MOLECULAR DYNAMICS

Molecular dynamics simulation of a classical molecular system of p atoms acting under a potential $U(\mathbf{q})$ involves numerical solution of the differential system arising from Newtonian dynamics,[14,15]

a)Author to whom correspondence should be addressed. Tel.: (919) 684-8064. FAX: (919) 684-8594. Electronic mail: schmidler@stat.duke.edu.

$$\dot{\mathbf{q}}_i = \frac{\mathbf{p}_i}{m_i}, \quad \dot{\mathbf{p}}_i = -\frac{\partial U(\mathbf{q}_i)}{\partial \mathbf{q}_i}. \tag{1}$$

This system yields trajectories in the phase space $\mathcal{X}=(\mathbf{q},\mathbf{p}) \in \mathbb{R}^{2pd}$ of configurations $\mathbf{q}$ and associated momenta $\mathbf{p}$. For macromolecules and standard molecular mechanics potentials, the result is a stiff system of tens of thousands of tightly coupled second-order ODEs, a many-body problem which cannot be solved analytically.

In practice this continuous time deterministic dynamical system is solved by numerical integration, yielding a discrete time deterministic dynamical system. A common choice in molecular simulation[16,17] is the use of the "leap-frog" numerical integrator, so-called because the momenta are calculated on half timesteps and the positions on full timesteps,

$$\begin{aligned} \mathbf{q}(t+\Delta t) &= \mathbf{q}(t) + \frac{\mathbf{p}(t+\Delta t/2)}{m}\Delta t, \\ \mathbf{p}(t+\Delta t/2) &= \mathbf{p}(t-\Delta t/2) + F(\mathbf{q}(t))\Delta t. \end{aligned} \tag{2}$$

However, limits on the stepsize Δt required by the numerical approximation (2) rarely permit the simulation of macromolecules on time-scales sufficient to observe important conformational changes, such as protein folding, ligand binding, and complex formation.

Replica-exchange molecular dynamics[1] is an application of the parallel tempering method[2] to deterministic molecular dynamics (MD) simulation, intended to speed up simulations by enabling the crossing of energy barriers. Both REMD and parallel tempering run multiple parallel simulations at a sequence of increasing temperatures $(T_0=T,\ldots,T_k)$ and intermittently attempt to swap simulations between temperatures. However, where parallel tempering uses stochastic component simulations based on Markov chains, the REMD algorithm instead runs multiple *deterministic* isothermal MD simulations. Then every r steps, two chains i and j are randomly chosen (or i random and $j=i+1$), and the proposed swap accepted with probability given by the Metropolis ratio,

$$\min\left\{1, \frac{\pi_{T_j}(\mathbf{q}_i,\mathbf{p}_i)\pi_{T_i}(\mathbf{q}_j,\mathbf{p}_j)}{\pi_{T_i}(\mathbf{q}_i,\mathbf{p}_i)\pi_{T_j}(\mathbf{q}_j,\mathbf{p}_j)}\right\},$$

where $\pi_i(\mathbf{q},\mathbf{p})$ is the Boltzmann distribution (canonical ensemble) for replica i at temperature T_i,

$$\begin{aligned} \pi_{T_i}(\mathbf{q},\mathbf{p}) &= Z_{T_i}^{-1} e^{-(1/k_B T_i)\mathcal{H}(\mathbf{q},\mathbf{p})}, \\ Z_T &= \int_{\mathcal{X}} e^{-(1/k_B T)\mathcal{H}(\mathbf{q},\mathbf{p})} d\mathbf{q}d\mathbf{p}, \end{aligned} \tag{3}$$

where $\mathcal{H}(\mathbf{q},\mathbf{p})=U(\mathbf{q})+\Sigma_i\|\mathbf{p}_i\|^2/2m_i$ is the Hamiltonian given by the sum of potential and kinetic energies, and k_B is Boltzmann's constant. The result is a stochastic dynamical system on $\mathcal{X}^*=\mathbb{R}^{2pdk}$, whose properties we wish to consider.

III. ERGODICITY AND INVARIANCE IN MOLECULAR SIMULATION

An important application of molecular simulation techniques in practice, as well as a key step in evaluating and improving forcefields,[6] is the calculation of experimental observables via ensemble averages,

$$\langle f \rangle = \int_{\mathcal{X}} f(\mathbf{q},\mathbf{p})\pi(\mathbf{q},\mathbf{p})d\mathbf{q}d\mathbf{p}.$$

A critical requirement of a (deterministic or stochastic) simulated molecular dynamical system is therefore that it be *ergodic*, namely, that limiting long-run time averages equal averages over the configurational ensemble,

$$\lim_{t\to\infty}\frac{1}{t}\int_0^t f(\mathbf{q}(s),\mathbf{p}(s))ds = \langle f \rangle,$$

or in practice, we require for the time-discretized dynamics given by the iterated mapping S that

$$\lim_{n\to\infty}\frac{1}{n}\sum_{k=1}^{n} f(S^k(\mathbf{q}_0,\mathbf{p}_0)) = \langle f \rangle, \tag{4}$$

for all integrable functions f. If Eq. (4) holds, time-averaged quantities computed from sufficiently long simulation trajectories can be used to compute thermodynamic properties of the system such as equilibrium constants and free energies, transition rates, and other experimental observables.

Ergodicity is often taken as an *assumption* in molecular simulation, but we will show that Eq. (4) does not hold for many simulation techniques in common use. It is important to note that although the ensemble (3) is completely determined by the potential (forcefield) U, a dynamical simulation which fails to satisfy Eq. (4) will not properly generate this ensemble and therefore not accurately reflect the forcefield.

It is well known[18,19] that dynamical systems exhibit such ergodic limiting behavior if and only if they are both *invariant* (or *measure-preserving*), and *irreducible*, with respect to π. A transformation[20] S on $\mathcal{X}$ is π-invariant if $\pi(S^{-1}A)=\pi(A)$ for every $A\subset\mathcal{X}$, or equivalently, if for any $f \in L_1(\pi)$,

$$\int_{\mathcal{X}} f(x)d\pi = \int_{\mathcal{X}} f(S(x))d\pi. \tag{5}$$

S is *irreducible* if it can, and eventually does, reach any state in the system from any other state. If S is both measure-preserving and irreducible, then it is ergodic and Eq. (4) holds.[20] Formally, S is *ergodic* on $(\mathcal{X},\pi)$ if $A\subset\mathcal{X}$ satisfies $S^{-1}A=A$ if and only if $\pi(A)=0$ or 1; equivalently, for $\pi(A)>0$ then $\cup_{n=1}^{\infty}S^{-n}A=\mathcal{X}$, and for $\mu(A)>0$ and $\mu(B)>0$, then $\mu(S^{-n}A\cap B)>0$ for some $n\geqslant 1$. Informally, invariance means that the dynamics has π as an equilibrium, and ergodicity guarantees the equilibrium is unique and the dynamics will converge to π from any starting point.[20]

A. Ergodicity and invariance of replica exchange

Write the discretized dynamics of MD at fixed temperature T as a mapping on phase space $S_T:\mathcal{X}\to\mathcal{X}$ taking posi-

tions and momenta at time t to new positions and momenta at time $t+\Delta t$. Then REMD can be written as a mapping $S^*:\mathcal{X}^*\to\mathcal{X}^*$ formed as a composition $S^*=S_1^r\circ S_2$ where S_1 is a block-diagonal mapping given by the direct sum $S_1=\oplus_{i=1}^k S_{T_i}$, and S_2 is the stochastic temperature swap given by the transition kernel,

$$S_2(\mathbf{x},A)=\frac{1}{k^2}\sum_{i,j}\mathbf{1}_A((i,j)\mathbf{x})\rho(\mathbf{x},(i,j)\mathbf{x}) + \mathbf{1}_A(\mathbf{x})\left[1-\frac{1}{k^2}\sum_{i,j}\rho(\mathbf{x},(i,j)\mathbf{x})\right],$$

where $\mathbf{x}=((\mathbf{q}_{T_1},\mathbf{p}_{T_1}),\ldots,(\mathbf{q}_{T_n},\mathbf{p}_{T_n}))$ and we use the transposition notation $(i,j)\mathbf{x}$ to denote the state after swapping configurations between temperatures i and j, which is accepted or rejected according to the Metropolis criteria,[21]

$$\rho(\mathbf{x},(i,j)\mathbf{x})=\min\left\{1,\frac{\pi_{T_i}(\mathbf{x}_j)\pi_{T_j}(\mathbf{x}_i)}{\pi_{T_i}(\mathbf{x}_i)\pi_{T_j}(\mathbf{x}_j)}\right\}.$$

By construction, ρ ensures the swapping step S_2 is reversible with respect to the joint Boltzmann distribution,

$$\pi(\mathbf{x})=\prod_{i=1}^{k}\pi_{T_i}(\mathbf{q}_i,\mathbf{p}_i),$$

and thus leaves the product measure π invariant. It follows that the replica-exchange dynamics S^* leave $\pi(\mathbf{x})$ invariant on the product space $\mathcal{X}^k$ if and only if the isothermal dynamics S_{T_j} leave $\pi_{T_j}(\mathbf{q}_j,\mathbf{p}_j)$ invariant for each temperature T_j. In Sec. V we show that one simulation method commonly used for biomolecules fails to do so.

Because Eq. (3) is strictly positive for all $T>0$, S^* is ergodic if any of the individual S_{T_i}'s are ergodic. On the other hand, if the S_{T_i} are reducible for all $i=1,\ldots,k$, the combined dynamics may or may not be ergodic due to swapping, the ergodicity of S^* must be verified. In Sec. V we show that two common isothermal dynamics simulation methods, Nosé–Hoover and Nosé–Poincaré, fail to be ergodic and that REMD using these methods also fails to be ergodic. In other words, if the underlying constant-temperature dynamics associated with individual replicas are nonergodic, swapping them by replica exchange is unlikely to fix the problem. In Sec. VI we provide a simple fix for this problem.

If S^* is π-invariant and ergodic, then by Eq. (4) the individual temperature trajectories $(\mathbf{q}_i^{(t)},\mathbf{p}_i^{(t)})$ of an REMD simulation converge to ensemble averages under the constant temperature (canonical) Boltzmann ensemble for each T_i, and in particular for T_0, the temperature of interest.

IV. HAMILTONIAN DYNAMICS AND SYMPLECTIC INTEGRATORS

Most of the dynamical systems used in MD and REMD simulation which we consider satisfy Eq. (5) for the Boltzmann probability measure $\pi_H(\mathbf{q},\mathbf{p})=\delta(\mathcal{H}(\mathbf{q},\mathbf{p})-\mathcal{H}(\mathbf{q}_0,\mathbf{p}_0))$, by virtue of forming *Hamiltonian systems*. A Hamiltonian system is a differential system of the form

$$\frac{d\mathbf{q}}{dt}=\frac{\partial\mathcal{H}}{\partial\mathbf{p}},\quad \frac{d\mathbf{p}}{dt}=-\frac{\partial\mathcal{H}}{\partial\mathbf{q}}.$$

Newtonian dynamics (1) is a Hamiltonian system, with Hamiltonian $\mathcal{H}(\mathbf{x})=U(\mathbf{q})+\Sigma_i\|\mathbf{p}_i\|^2/2m_i$, and the corresponding π is the *microcanonical* (or constant energy) ensemble. Any Hamiltonian system conserves its associated Hamiltonian $\mathcal{H}$,

$$\frac{d\mathcal{H}}{dt}=\frac{\partial\mathcal{H}}{\partial\mathbf{q}}\frac{d\mathbf{q}}{dt}+\frac{\partial\mathcal{H}}{\partial\mathbf{p}}\frac{d\mathbf{p}}{dt}=\frac{\partial\mathcal{H}}{\partial\mathbf{q}}\frac{\partial\mathcal{H}}{\partial\mathbf{p}}+\frac{\partial\mathcal{H}}{\partial\mathbf{p}}\left(-\frac{\partial\mathcal{H}}{\partial\mathbf{q}}\right)=0,$$

and, therefore,

$$\begin{aligned}\int_{\mathcal{X}}f(\mathbf{q},\mathbf{p})d\pi&=\int_{\mathcal{X}}f(\mathbf{q},\mathbf{p})\frac{1}{Z}e^{-\mathcal{H}(\mathbf{q},\mathbf{p})/(k_BT)}d\mathbf{q}d\mathbf{p}\\&=\int_{\mathcal{X}}f(S(\mathbf{q},\mathbf{p}))\frac{1}{Z}e^{-\mathcal{H}(S(\mathbf{q},\mathbf{p}))/(k_BT)}|J_s|d\mathbf{q}d\mathbf{p}\\&=\int_{\mathcal{X}}f(S(\mathbf{q},\mathbf{p}))\frac{1}{Z}e^{-\mathcal{H}(\mathbf{q},\mathbf{p})/(k_BT)}|J_s|d\mathbf{q}d\mathbf{p}\\&=\int_{\mathcal{X}}f(S(\mathbf{q},\mathbf{p}))d\pi.\end{aligned}$$

Therefore, to be π-invariant, S must have Jacobian equal to unity. Liouville's theorem states that this holds for any Hamiltonian dynamics—namely, that Hamiltonian dynamics are volume (or *Lebesgue measure*) preserving.[22] Note that often S may not be ergodic on π_H, and so from Sec. III still does not generate the microcanonical ensemble, i.e., does not satisfy Eq. (4).

A. Symplectic integrators

A key point is that the properties of Sec. III—invariance and ergodicity—must hold not only for the theoretical continuous time dynamical system, but also for the time-discretized dynamics obtained in practice by application of numerical integration on a computer. In practice, the numerical integrators chosen for MD, such as the leap-frog integrator (2), are chosen to be *symplectic*,[23] a property that implies phase-space volume preserving. For any $\Delta t>0$, however, they only approximately conserve the Hamiltonian $\mathcal{H}$. (The hybrid Monte Carlo modifications given in Sec. VI corrects for this.)

It is easily checked that the leap-frog integrator (2) is volume preserving, by writing

$$S_a:\quad(\mathbf{q},\mathbf{p})\mapsto(\mathbf{q}',\mathbf{p}')=(\mathbf{q},\mathbf{p}+F(\mathbf{q})\Delta t),$$

$$S_b:\quad(\mathbf{q}',\mathbf{p}')\mapsto(\mathbf{q}'',\mathbf{p}'')=\left(\mathbf{q}'+\frac{\mathbf{p}'}{m}\Delta t,\mathbf{p}'\right),$$

with

$$J_{S_a}=\begin{vmatrix}1&0\\F'(\mathbf{q})\Delta t&1\end{vmatrix}=1,\quad J_{S_b}=\begin{vmatrix}1&(1/m)\Delta t\\0&1\end{vmatrix}=1.$$

However, replica-exchange dynamics relies on *isothermal* (constant temperature) dynamics to generate the canonical ensemble, rather than the microcanonical (constant energy)

ensemble generated by Newtonian dynamics. Isothermal dynamics requires modified Hamiltonians and specialized integrators. We will see that not all of the numerical integrators used in such dynamics are in fact volume-perserving; while in other cases the underlying dynamics fail to be ergodic.

V. ISOTHERMAL MOLECULAR DYNAMICS

Replica-exchange molecular dynamics relies on the use of *isothermal* (constant temperature) or *canonical ensemble* molecular dynamics simulations at each level of the temperature ladder. The original formulation[1] of REMD utilized the Berendsen heat-bath algorithm[24] to achieve isothermal dynamics, and this has been standard practice in REMD simulations.[6,25–29] More recently, the Nosé–Hoover thermostat algorithm has also been applied for this purpose.[29] We briefly review these and related methods for performing deterministic isothermal dynamics. Our focus is on viewing these algorithms with respect to the invariance and irreducibility properties defined in Sec. III; as we will see, *all* of these algorithms fail to yield an ergodic replica-exchange dynamics.

A. Velocity rescaling and the Berendsen heat bath

By far the most commonly used algorithm for constant temperature MD of biomolecules is the Berendsen heat bath,[24] due to its ease of implementation and availability in standard software packages.[30–32] In this approach, the system is weakly coupled to a heat bath by rescaling the momenta after each step to adjust the temperature, at rate proportional to the difference between current and target temperatures,

$$\frac{dT(t)}{dt} = \frac{1}{\tau}(T - T(t)).$$

This amounts to convolving the mapping $R:(\mathbf{q},\mathbf{p}) \mapsto (\mathbf{q},\lambda\mathbf{p})$ with the (Δt-discretized) dynamics, where

$$\lambda^2 = 1 + \frac{\Delta t}{\tau}\left(\frac{T}{\hat{T}(t)} - 1\right), \quad \hat{T}(t) = \left(\frac{3p}{2}k_B T\right)^{-1} \sum_{i=1}^{p} \frac{\|\mathbf{p}_i\|^2}{2m_i}.$$

However, it is easily seen (and well known, see, e.g., Ref. 16) that this mapping is not invariant under the canonical distribution

$$\begin{aligned}
&\int_{\mathcal{X}} f(\mathbf{q}',\mathbf{p}')d\pi(\mathbf{q}',\mathbf{p}') \\
&= \int_{\mathcal{X}} f(\mathbf{q}',\mathbf{p}')\frac{e^{-\mathcal{H}(\mathbf{q}',\mathbf{p}')/(k_B T)}}{Z}d\mathbf{q}'d\mathbf{p}' \\
&= \int_{\mathcal{X}} f(\mathbf{q},\lambda\mathbf{p})\frac{e^{-\mathcal{H}(\mathbf{q},\lambda\mathbf{p})/(k_B T)}}{Z}\lambda d\mathbf{q}d\mathbf{p} \\
&\neq \int_{\mathcal{X}} f(\mathbf{q},\mathbf{p})d\pi(\mathbf{q},\mathbf{p}).
\end{aligned}$$

In addition, the resulting dynamics are clearly not time-reversible. Thus the Berendsen heat bath approach to isothermal MD does not generate the canonical ensemble (although Morishita[33] argues that it approximately preserves certain properties). Since we saw in Sec. III that REMD is π-invariant f and only if each replica is π_T-invariant, REMD fails to generate the canonical ensemble when implemented via the Berendsen algorithm. Given the extensive use of the Berendsen heat bath in MD and REMD simulations,[1,6,25–29] this is a source of some concern. In Sec. VII, we demonstrate significant failures of the Berendsen-based REMD algorithm on examples.

B. Extended Lagrangian methods

1. Nosé–Hoover thermostat

An alternative method for isothermal dynamics based on an extended Lagrangian was introduced by Nosé,[34] and reformulated by Hoover.[35] This approach has been used as an alternative to the Berendsen thermostat to generate constant temperature dynamics for REMD.[29] Nosé adds an additional coordinate s, rescaling time to $dt' = dt/s$, and introducing the augmented Hamiltonian,

$$\mathcal{H}_{\text{Nosé}} = U(\mathbf{q}) + \sum_i \frac{\|\mathbf{p}_i\|^2}{2m_i s^2} + \frac{p_s^2}{2Q} + g k_B T \ln s, \tag{6}$$

where s is a time-scale variable with conjugate momentum p_s, Q is a parameter of dimension energy $\times$ time^2 which behaves like a mass for the motion of s, and g is the degrees of freedom plus one. The equations of motion then become

$$\frac{d\mathbf{q}_i}{dt'} = \frac{\partial \mathcal{H}}{\partial \mathbf{p}_i} = \frac{\mathbf{p}_i}{m_i s^2}, \quad \frac{d\mathbf{p}_i}{\partial t'} = -\frac{\partial \mathcal{H}}{\partial \mathbf{q}_i} = -\frac{\partial}{\partial \mathbf{q}_i}U(\mathbf{q}),$$

$$\frac{ds}{dt'} = \frac{\partial \mathcal{H}}{\partial p_s} = \frac{p_s}{Q},$$

$$\frac{dp_s}{dt'} = -\frac{\partial \mathcal{H}}{\partial s} = \left(\sum_i \frac{\|\mathbf{p}_i\|^2}{m_i s^2} - gkT\right) \Big/ s.$$

As with all Hamiltonian systems, these dynamics preserve the Hamiltonian $\mathcal{H}_{\text{Nosé}}$,

$$\begin{aligned}
\frac{d\mathcal{H}}{dt'} &= \frac{\partial \mathcal{H}}{dp_s}\frac{dp_s}{dt'} + \frac{\partial \mathcal{H}}{\partial s}\frac{ds}{dt'} + \sum_i \left(\frac{\partial \mathcal{H}}{\partial \mathbf{q}_i}\frac{\partial \mathbf{q}_i}{\partial t} + \frac{\partial \mathcal{H}}{\partial \mathbf{p}_i}\frac{d\mathbf{p}_i}{dt'}\right) \\
&= \frac{\partial \mathcal{H}}{\partial p_s}\left(-\frac{\partial \mathcal{H}}{\partial s}\right) + \frac{\partial \mathcal{H}}{\partial s}\left(\frac{\partial \mathcal{H}}{\partial p_s}\right) \\
&\quad + \sum_i \left(\frac{\partial \mathcal{H}}{\partial \mathbf{q}_i}\left(\frac{\partial \mathcal{H}}{\partial \mathbf{p}_i}\right) + \frac{\partial \mathcal{H}}{\partial \mathbf{p}_i}\left(-\frac{\partial \mathcal{H}}{\partial \mathbf{q}_i}\right)\right) = 0
\end{aligned}$$

and Nosé showed that the microcanonical ensemble in this augmented phase-space yields the canonical ensemble for $(\mathbf{q},\mathbf{p}/s)$, independent of choice of Q and the initial value of $\mathcal{H}_{\text{Nosé}}$. However, because time is scaled by s which changes as the differential equation evolves, the system is not convenient for computation. Hoover[35] remedied this problem by modifying the Nosé dynamics to create a non-Hamiltonian dynamics. The system simplifies to three equations:

$$\dot{\mathbf{q}}_i = \frac{\mathbf{p}_i}{m_i}, \quad \dot{\mathbf{p}}_i = -\frac{\partial}{\partial \mathbf{q}_i} U(\mathbf{q}) - \zeta \mathbf{p}_i, \quad \dot{\zeta} = \frac{1}{Q}\left(\sum_i \frac{\mathbf{p}_i}{m_i} - gkT\right), \tag{7}$$

where $g=N_f$ is degrees of freedom of the real system, compared to $g=N_f+1$ in the Nosé system. Although the Nosé–Hoover system is no longer Hamiltonian, it conserves the *extended energy*,

$$E_{\text{ext}}(\mathbf{q},\mathbf{p},\zeta) = U(\mathbf{q}) + \sum_i \frac{\|\mathbf{p}_i\|^2}{2m_i} + \frac{Q\zeta^2}{2}, \tag{8}$$

and Hoover[35] argues that it also conserves the associated Boltzmann distribution,

$$\pi(\mathbf{q},\mathbf{p},\zeta) = Z^{-1} e^{-(1/k_B T) E_{\text{ext}}(\mathbf{q},\mathbf{p},\zeta)},$$

by use of the conservation of mass or continuity equation $d\pi/dt = \partial\pi/\partial t + \nabla\cdot(\pi\mathbf{u}) = 0$ where $\mathbf{u} = [d\mathbf{q}/dt, d\mathbf{p}/dt, d\zeta/dt]$ is the "fluid" velocity. However, although the Nosé–Hoover dynamics conserve the density π, they do not preserve the underlying measure (phase-space volume) and so are not symplectic. To see this consider $\lim_{t\to 0}(|V(t)|-|V(0)|)/t$ which goes to zero for Hamiltonian dynamics by Liouville's theorem,[22] but not for Nosé–Hoover dynamics. Let $\mathbf{x} = (\mathbf{q},\mathbf{p})$ and define $g^t(\mathbf{x}) = (\mathbf{q},\mathbf{p}) + (\dot{\mathbf{q}},\dot{\mathbf{p}})t + O(t^2)$. Then,

$$\begin{aligned} |V(t)| &= \int_{V(0)} \det\left(\frac{\partial g^t(\mathbf{x})}{\partial \mathbf{x}}\right) d\mathbf{q}d\mathbf{p} \\ &= \int_{V(0)} [1 - \zeta t + O(t^2)] d\mathbf{q}d\mathbf{p} \\ &= V(0)(1 - \zeta t) + O(t^2). \end{aligned}$$

We can then see that $\lim_{t\to 0}(|V(t)|-|V(0)|)/t = -\zeta V(0) \neq 0$, so the volume of the phase-space is not preserved, as recognized by Hoover.[35] But then the Nosé–Hoover dynamics are not π-invariant, since

$$\begin{aligned} &\int_{\mathcal{X}} f(\mathbf{x}') d\pi(\mathbf{x}') \\ &= \int_{\mathcal{X}} f(\mathbf{q}',\mathbf{p}',\zeta') \frac{e^{-[U(\mathbf{q}')+\Sigma_i \|\mathbf{p}_i'\|^2/2m_i + Q\zeta'^2/2]/(k_B T)}}{Z Z_\zeta} d\mathbf{q}' d\mathbf{p}' d\zeta' \\ &= \int_{\mathcal{X}} f(\mathbf{q},\mathbf{p},\zeta) \frac{e^{-[U(\mathbf{q})+\Sigma_i (\|\mathbf{p}_i\|^2/2m_i) + Q\zeta^2/2]/(k_B T)}}{Z Z_\zeta} |J_T| d\mathbf{q}d\mathbf{p}d\zeta \\ &\neq \int_{\mathcal{X}} f(\mathbf{x}) d\pi(\mathbf{x}). \end{aligned}$$

Specialized integrators have been developed for Nosé–Hoover dynamics simulation. The method of Winkler *et al.*[36] addresses some shortcomings of others and is described in Appendix A 1, but is also not symplectic. Of greater concern is that the underlying continuous time Nosé–Hoover dynamics themselves fail to be irreducible, as observed empirically by Hoover[35] and noted by many others.[16,33,37] As Nosé–Hoover has been used in REMD simulation,[29] we show in Sec. V C 1 that REMD using Nosé–Hoover dynamics also fails to be ergodic; i.e., the stochastic swapping of introduced by replica-exchange is not sufficient to achieve irreducibility.

2. Nosé–Poincaré Hamiltonian

To circumvent the difficulties which arise from the non-Hamiltonian nature of the Nosé–Hoover dynamics, Bond *et al.*[38] constructed a Poincaré time transformation of the original Nosé system. The Poincaré transformation of the Nosé Hamiltonian (6) yields a new Hamiltonian,

$$\mathcal{H} = s\Delta\mathcal{H} = s\left(U(\mathbf{q}) + \sum_i \frac{\|\mathbf{p}_i\|^2}{2m_i s^2} + \frac{p_s^2}{2Q} + gkT \ln s - \mathcal{H}_0\right), \tag{9}$$

where $\Delta\mathcal{H} = \mathcal{H}_{\text{Nosé}} - \mathcal{H}_0$ and $\mathcal{H}_0$ is the initial value of $\mathcal{H}$ at time $t=0$. The resulting Hamiltonian system is then

$$\frac{d\mathbf{q}_i}{dt} = \frac{\partial \tilde{\mathcal{H}}}{\partial \mathbf{p}_i} = \frac{\mathbf{p}_i}{m_i s}, \quad \frac{d\mathbf{p}_i}{dt} = -\frac{\partial \tilde{\mathcal{H}}}{\partial \mathbf{q}_i} = -s\frac{\partial}{\partial \mathbf{q}_i} U(\mathbf{q}),$$

$$\frac{ds}{dt} = \frac{\partial \tilde{\mathcal{H}}}{\partial p_s} = \frac{s p_s}{Q},$$

$$\frac{dp_s}{dt} = -\frac{\partial \tilde{\mathcal{H}}}{\partial s} = \sum_i \frac{\|\mathbf{p}_i\|^2}{m_i s^2} - gkT + \Delta\mathcal{H}(\mathbf{q},\mathbf{p},s,p_s),$$

and $\mathcal{H}_0$ is chosen so that initially $\Delta\mathcal{H}=0$. Since this is a Hamiltonian system, it conserves the Hamiltonian (9) and by Liouville's theorem is volume-preserving. Bond *et al.*[38] show that if the Nosé–Poincaré dynamics are ergodic, they also generate the correct marginal Boltzmann distribution of $(\mathbf{p},\mathbf{q})$ [Eq. (3)]. Nosé[39] gives an explicit, time-reversible, symplectic integrator for the Nosé–Poincaré dynamics, which is used in Sec. VII and described in Appendix A 2.

C. Failure of ergodicity in REMD using isothermal dynamics

We showed in Sec. V A that the Berendsen thermostat fails to preserve the Boltzmann measure, and therefore by definition (Sec. III) isothermal dynamics simulations using Berendsen, and REMD simulations with Berendsen-controlled temperatures, fail to be ergodic. In this section we demonstrate that REMD simulations using both Nosé–Hoover and Nosé–Poincaré dynamics also fail to be ergodic, due to reducibility in phase space. Significant attention has been paid in the literature to empirical evidence of ergodicity or lack thereof for these methods, including new variants (chains) introduced to "enhance ergodicity." Here, we show rigorously that these methods fail to be ergodic, removing any ambiguity. The practical impact of these failures are demonstrated on several examples in Sec. VII.

1. REMD with Nosé–Hoover is not ergodic

To show that replica exchange using Nosé–Hoover dynamics fails to be ergodic, we first demonstrate that a single

Nosé–Hoover dynamics fails to be ergodic. This was observed by Hoover[35] and has since been noted by many others.[16,33,37]

Lemma 5.1: *The Nosé–Hoover differential system (7) with unbounded potential energy* $|U(\mathbf{q})|$ *is not ergodic under the Boltzmann measure*.

Proof: Define the phase-space subsets,

$$A = \left\{ (\mathbf{q},\mathbf{p},\zeta): U(\mathbf{q}) + \sum_i \frac{\|\mathbf{p}_i\|^2}{2m_i} < a, \frac{Q\zeta^2}{2} < b \right\} \quad \text{and}$$

$$B = \left\{ (\mathbf{q},\mathbf{p},\zeta): U(\mathbf{q}) + \sum_i \frac{\|\mathbf{p}_i\|^2}{2m_i} > a+b \right\},$$

for some constants a, b, and note that A and B both have positive Boltzmann measure. Then Nosé–Hoover dynamics cannot reach A from B, since the mapping S_{NH} preserves the extended energy (8), and so for any $(\mathbf{p},\mathbf{q},\zeta) \in A$ and $n \geqslant 1$ we have

$$E_{\mathrm{ext}}(S_{\mathrm{NH}}^{-n}(\mathbf{p},\mathbf{q},\zeta)) = U(\mathbf{q}) + \sum_i \frac{\|\mathbf{p}_i\|^2}{2m_i} + \frac{Q\zeta^2}{2} < a+b,$$

and since $Q\zeta^2/2 \geqslant 0$, we have $\pi(B \cap S_{\mathrm{NH}}^{-n} A) = 0$. □

We can now show that REMD using Nosé–Hoover dynamics fails to be ergodic, by showing that for any set of initial configurations $\{(\mathbf{q}_{T_i}^0, \mathbf{p}_{T_i}^0, \zeta_{T_i}^0)\}$, there exists a set B with $\pi_{T_i}(B) > 0$ that no trajectory can reach.

Theorem 5.2: *REMD using Nosé–Hoover dynamics with unbounded potential energy* $|U(\mathbf{q})|$ *is not ergodic under the Boltzmann measure*.

Proof: Given any set of initial configurations $\{\mathbf{x}_{T_i}^0 = (\mathbf{q}_{T_i}^0, \mathbf{p}_{T_i}^0, \zeta_{T_i}^0)\}_{i=1}^k$, let $a = \max_i \{U(\mathbf{q}_{T_i}^0) + \Sigma_j \|\mathbf{p}_{T_i,j}^0\|^2/2m_j\}$, and $b = \max_i \{Q(\zeta_{T_i}^0)^2/2\}$. Define sets $A = \{\mathbf{x}: E_{\mathrm{ext}}(\mathbf{x}) < a+b\}$ and $B = \{\mathbf{x}: U(\mathbf{q}) + \Sigma_i \|\mathbf{p}_i\|^2/2m_i > a+b\}$. Then $\mathbf{x}_{T_i}^0 \in A$ for all T_i, and by Lemma 5.1 the Nosé–Hoover mapping S_{T_i}, at any temperature T_i cannot reach B from A since $\pi_{T_i}(S_{T_i}^{-n} A \cap B) = 0$ for all n. But the temperature swap S_2 does not change the value of E_{ext} for any configuration, since T_i does not appear in Eq. (8). Now define sets $A^* = \{\{\mathbf{x}_{T_i}\}_{i=1}^k : E_{\mathrm{ext}}(\mathbf{x}_{T_i}) < a+b \forall_i\}$ and $B^* = \{\{\mathbf{x}_{T_i}\}_{i=1}^k : U(\mathbf{q}_{T_i}) + \Sigma_j \|\mathbf{p}_{T_i,j}\|^2/2m_j > a+b \forall i\}$. Then $\{\mathbf{x}_{T_i}^0\} \in A^*$, and neither the Nosé–Hoover dynamics nor the temperature swap enable any chain to move from A to B, so $\pi(B^* \cap S^{*-n} A^*) = 0$ for all n. □

2. Nosé–Hoover chains

As mentioned in Sec. V C 1, the failure of Nosé–Hoover to be ergodic is well known. Martyna *et al.*[37] introduced a modification called *Nosé–Hoover chains*, which adds on M chains so that the conserved quantity becomes

$$\sum_{i=1}^{p} \frac{\|\mathbf{p}_i\|^2}{2m_i} + U(\mathbf{q}) + \sum_{i=1}^{M} \frac{Q_i \zeta_i^2}{2} \tag{10}$$

where m_i, $Q_i \geqslant 0$ for all i. However, although the addition of the ζ_i's increases the range of accessible potential energies (adding REMD replicas has a similar effect in this regard), this range remains bounded by the initial values of the ζ_i's and $\mathbf{p}_i$'s.

Corollary 5.3: *Nosé–Hoover chains as defined by Martyna et al.*[37] *are not ergodic.*

Proof: The sum defined by $\Sigma_{i=1}^M (Q_i \zeta_i^2/2)$ is always positive if $Q_i > 0$ for all i, so the argument from Lemma 5.1 holds. □

Thus, for unbounded energy functions U such as commonly used molecular mechanics forcefields, neither Nosé–Hoover nor Nosé-Hoover chains are truly ergodic, as one can always find a value of the potential energy that cannot be reached. In addition if the system fails to be ergodic in this way, it may fail in others also.

3. REMD with Nosé–Poincaré is not ergodic

Similarly, we will show that the Nosé–Poincaré dynamics are not ergodic, and that this implies that REMD using Nosé–Poincaré isothermal components fails to be ergodic.

Lemma 5.4: *Neither the Nosé–Poincaré method*[38] *nor the original Nosé method is ergodic on* $\mathcal{Q} \times \mathcal{P}$.

Proof: The Nosé–Poincaré system is Hamiltonian and thus preserves the Hamiltonian (9) given by $\tilde{\mathcal{H}} = s(\mathcal{H}_{\mathrm{Nosé}} - \mathcal{H}_0)$. Because $\mathcal{H}_0$ is a constant chosen such that the initial value of $\tilde{\mathcal{H}}$ is zero, the value of $\mathcal{H}_{\mathrm{Nosé}}$ is also preserved by Nosé–Poincaré dynamics. The following argument uses only the preservation of $\mathcal{H}_{\mathrm{Nosé}}$ and so applies to both Nosé–Poincaré and Nosé dynamics. Define two sets,

$$A = \left\{ (\mathbf{q},\mathbf{p},s,p_s): \quad |U(\mathbf{q})| < \epsilon; \quad \sum_i \frac{\|\mathbf{p}_i\|^2}{2m_i} < \epsilon; \right.$$
$$\left. \frac{p_s^2}{2Q} < \alpha; \quad |gkT \ln s| < \beta \right\},$$

$$B = \left\{ (\mathbf{q},\mathbf{p},s,p_s): \quad U(\mathbf{q}) > V; \quad \sum_i \frac{\|\mathbf{p}_i\|^2}{2m_i} > 1 \right\},$$

with V chosen as follows. Note that $|gkT \ln s| < \beta$ implies $s^{-2} < e^{2\beta/gkT}$ so for $(\mathbf{q},\mathbf{p},s,p_s) \in A$,

$$\sum_i \frac{\|\mathbf{p}_i\|^2}{2m_i s^2} < \epsilon e^{2\beta/gkT} \triangleq \gamma,$$

and so V can be chosen to satisfy $V > \alpha + \beta + \gamma + \epsilon - (gkT/2) \times [1 + \ln 2 - \ln(gkT)]$. Then a dynamics preserving $\mathcal{H}_{\mathrm{Nosé}}$ and starting from A cannot reach B, because for potential energy $U(\mathbf{q})$ to increase to V requires

$$\sum_i \frac{\|\mathbf{p}_i\|^2}{2m_i s^2} + \frac{p_s^2}{2Q} + gkT \ln s < \alpha + \beta + \gamma - V.$$

To see that this cannot occur, let $c = gkT$ and notice that in the set B,

$$\sum_i \frac{\|\mathbf{p}_i\|^2}{2m_i s^2} + \frac{p_s^2}{2Q} + c \ln s \geqslant \frac{1}{s^2} + c \ln s,$$

since $\Sigma_i \|\mathbf{p}_i\|^2/2m_i > 1$. Differentiation shows that $f(s) = 1/s^2 + c \ln s$ achieves a minimum of $(c/2)[1 + \ln 2 - \ln c]$ at $s = \sqrt{2/c}$, so for positive s,

$$\sum_i \frac{\|\mathbf{p}_i\|^2}{2m_i s^2} + \frac{p_s^2}{2Q} + gkT \ln s \geqslant \frac{gkT}{2}[1 + \ln 2 - \ln(gkT)]$$
$$> \alpha + \beta + \gamma - V.$$

Therefore preserving $\mathcal{H}_{\text{Nosé}}$ requires $U(\mathbf{q}) < V$, so set B can never be reached. □

Note that because Nosé–Poincaré is time-reversible, A cannot be reached from B either. Looking at the choice of sets used in the lemma, we see that if we are unable to choose an initial configuration with sufficiently low potential energy, *it may be impossible to reach the region including the minimum potential energy configuration* with Nosé–Poincaré or Nosé–Hoover dynamics. So the failure to be ergodic has significant practical consequences; we show examples where exactly this phenomenon occurs in Sec. VII. We conclude this section by showing that, as with Nosé–Hoover, the nonergodicity at individual temperatures translates to non-ergodicity of the replica-exchange dynamics as well.

Theorem 5.5: *REMD using Nosé–Poincaré dynamics is not ergodic for unbounded positive potential energy* $U(\mathbf{q}) > 0$.

Proof: Given initial configurations $\mathbf{x}_{T_i}^0 = (\mathbf{q}_{T_i}^0, \mathbf{p}_{T_i}^0, s_{T_i}^0, p_{s,T_i}^0)$ for $i = 1 \ldots k$, define constants

$$a = \max_i \{U(\mathbf{q}_{T_i}^0)\},$$

$$b = \max_{i,j} \left\{ \sum_j \frac{\|\mathbf{p}_{T_i,j}^0\|^2}{2m_j (s_{T_i}^0)^2} + \frac{(p_{s,T_i}^0)^2}{2Q} + gkT_j \ln s_{T_i}^0 \right\},$$

$$c = \min_{i,s} \left\{ \frac{1}{s^2} + gkT_i \ln s \right\},$$

and define the sets

$$A = \left\{ \mathbf{x}: \quad U(\mathbf{q}) < a; \quad \sum_i \frac{\|\mathbf{p}_i\|^2}{2m_i} + \frac{p_s^2}{2Q} + gkT_i \ln s < b \right\},$$

$$B = \left\{ \mathbf{x}: \quad U(\mathbf{q}) > k(a+b+c); \quad \sum_i \frac{\|\mathbf{p}_i\|^2}{2m_i} > 1 \right\}.$$

From the proof of Lemma 5.1, we can see that for any individual temperature, $\pi_{T_i}(B \cap S_{T_i}^{-n} A) = 0$ because the maximum possible value for $U(\mathbf{q})$ at any temperature is less than $a+b+c$. For Nosé–Poincaré dynamics, unlike for Nosé–Hoover dynamics, the conserved quantity depends on T_i. However, the total increase in potential energy over all replicas is bounded by $k(a+b+c)$ since $(a+b+c)$ is the maximum increase at any temperature due to conservation of the Hamiltonian. Thus for any individual replica the total increase in $U(\mathbf{q})$ is also bounded by $k(a+b+c)$. Now define the sets

$$A^* = \left\{ \{\mathbf{x}_{T_i}\}_{i=1}^k : U(\mathbf{q}_{T_i}) < a; \sum_j \frac{\|\mathbf{p}_{T_i,j}\|^2}{2m_j} + \frac{p_{s,T_i}{}^2}{2Q} + gkT_i \ln s_{T_i} < b \ \forall\, i \right\}.$$

$$B^* = \left\{ \{\mathbf{x}_{T_i}\}_{i=1}^k : U(\mathbf{q}_{T_i}) > n(a+b+c); \sum_j \frac{\|\mathbf{p}_{T_i,j}\|^2}{2m_j} > 1 \ \forall\, i \right\}.$$

For every T_i, we have $\pi_{T_i}(B \cap S_{T_i}^{-n} A) = 0$ and $\pi(B^* \cap S_2^{-n} A^*) = 0$, so we have $\pi(B^* \cap (S^{*-n} A^*) = 0)$. □

D. Nosé–Poincaré chains

Following the apparent success of chains in improving the behavior of Nosé–Hoover dynamics, chains have also been added to the Nosé–Poincaré integrator.[38,40,41] Unfortunately, as with the Nosé–Hoover chains, these methods which aim to "enhance ergodicity"[40] do not make the system ergodic. The general form of the Nosé–Poincaré chains introduced by Laird and Leimkuhler[40] have Hamiltonian $\mathcal{H} = s(\hat{\mathcal{H}} - \hat{\mathcal{H}}_0)$, where

$$\hat{\mathcal{H}} = \sum_{i=1}^{p} \frac{\|\mathbf{p}_i\|^2}{2m_i s^2} + U(\mathbf{q}) + gkT \ln s + \frac{\mathbf{p}_s^2}{2Q_s} + f(s, p_s, \sigma_i, p_{\sigma_i}). \tag{11}$$

Laird and Leimkuhler[40] introduce two chain methods, both using functions f that are strictly positive. However, since $\hat{\mathcal{H}} - \hat{\mathcal{H}}_0$ by conservation of the Hamiltonian, by Lemma 5.4 $(\hat{\mathcal{H}} - U(\mathbf{q}))$ has a minimum for any initial values of $\mathbf{q}$, $\mathbf{p}$, s, and p_s. Thus, for f positive U remains bounded above, and the dynamics are not ergodic. More recently, Leimkuhler and Sweet[41] use functions f that can be take both positive and negative values, so the above proof does not extend directly, and it remains unclear if the method can be ergodic.

VI. STOCHASTIC DYNAMICS

One alternative to deterministic molecular dynamics [Eq. (1)] is the use of stochastic dynamics, including hybrid Monte Carlo[42] and Langevin or Brownian dynamics,[43] where the stochastic element corresponds to solvent collisions/thermal fluctuation. In contrast to deterministic dynamics, establishing ergodicity of stochastic dynamics is generally considerably easier due to the probabilistic nature of individual transitions.

A. Metropolis correction and hybrid Monte Carlo

An alternative is to use deterministic dynamics simulations to generate *proposed* moves, which are then accepted or rejected according to an appropriate Metropolis-Hastings criteria.[21,44] The *hybrid Monte Carlo* (HMC) algorithm[42,45] simulates a Hamiltonian system at temperature T starting from initial position and momentum vectors $(\mathbf{q}_0, \mathbf{p}_0)$ via the following iteration:

(1) Generate a random momentum vector $\mathbf{p} \sim N(\mathbf{0}, (k_B T)\mathbf{I}_{3d})$, where $N(\mu, \Sigma)$ denotes the normal (Gaussian) distribution.
(2) Simulate L steps of MD using a time-reversible volume-preserving integrator to generate a proposed new state $(\mathbf{x}', \mathbf{p}')$

(3) Accept the proposed state $(\mathbf{q}',\mathbf{p}')$ with probability α, otherwise reject and remain at current state $(\mathbf{q},\mathbf{p})$, where $\alpha((\mathbf{q},\mathbf{p});(\mathbf{q}',\mathbf{p}'))=\min\{1,\exp(\Delta\mathcal{H}/k_BT)\}$ and $\Delta\mathcal{H}=\mathcal{H}(\mathbf{q},\mathbf{p})-\mathcal{H}(\mathbf{q}',\mathbf{p}')$.

The resulting stochastic process is $\pi_{\mathcal{H}}$-invariant as long as the dynamics are time reversible and volume preserving, as has been first argued[42,45] and then shown carefully.[46] In addition, the randomization of the momenta guarantees that the underlying stochastic process is ergodic, as we show below. Here, L must be chosen along with Δt to yield an appropriate acceptance rate.

Hybrid Monte Carlo can be viewed as introducing stochastic corrections to the deterministic dynamics, correcting for the lack of both invariance and irreducibility. The Metropolis acceptance provides an exact correction for the approximate conservation of the Hamiltonian arising from time discretization. Similarly, we show below that the randomization of momenta turns the reducible deterministic dynamics into an irreducible stochastic process.

The HMC construction applies for any time-reversible volume-preserving dynamics. When applied to microcanonical dynamics it yields the HMC algorithm of Duane *et al.*[42] In Sec. VII, we apply it to Nosé–Poincaré dynamics using the integrator in Appendix A 2, yielding a π-invariant ergodic algorithm due to the symplectic property of the Nosé–Poincaré dynamics and integrator. We also apply the HMC correction to the Berendsen-thermostat MD, which should be seen only as a heuristic correction for ergodicity but does not yield π-invariance, since the Berendsen heat bath is neither measure-preserving nor time reversible.

1. Ergodicity of hybrid Monte Carlo

Lemma 6.1: *Hybrid Monte Carlo using the leap-frog (2) or the Nosé–Poincaré (Appendix A 2) integrators is ergodic.*

Proof: Denote by S the one step integrator mapping, and let K_H denote the transition kernel associated with one step of HMC,

$$K_H((\mathbf{q},\mathbf{p}),\mathbf{A}) = \int_{\mathcal{P}} f(\tilde{\mathbf{p}})\mathbf{1}_A(S^L(\mathbf{q},\tilde{\mathbf{p}}))\alpha((\mathbf{q},\mathbf{p}),S^L(\mathbf{q},\mathbf{p}))d\tilde{\mathbf{p}} + \mathbf{1}_A((\mathbf{q},\mathbf{p})) \times\left[1-\int_{\mathcal{P}} f(\tilde{\mathbf{p}})\alpha((\mathbf{q},\tilde{\mathbf{p}}),S^L(\mathbf{q},\tilde{\mathbf{p}}))d\tilde{\mathbf{p}}\right],$$

where f denotes the multivariate normal density $N(\mathbf{0},(k_BT)\mathbf{I}_{3d})$. Liu[46] formalizes the argument outlined previously[42,45] to show that S being time reversible and volume preserving implies that K_H is π-invariant. Thus, we need only show that K_H is also irreducible.

For a π-invariant stochastic process to be irreducible (and hence ergodic), it suffices that it be ϕ-*irreducible* for some distribution ϕ.[47] That is, for every $A\subset\mathcal{X}$ with $\phi(A)>0$, there exists an n such that $K_H^n(\mathbf{x},\mathbf{A})>0$ for all $\mathbf{x}\in\mathcal{X}$. K is *strongly* ϕ-irreducible if this holds for $n=1$. We show that HMC is strongly ϕ-irreducible, first for $L=1$ MD step and then for general L.

Define the set $B=\{(\mathbf{q},\mathbf{p}):a<U(\mathbf{q})<b\}$ and let ϕ be the uniform distribution over B. Then for any measurable $A\subseteq B$ and $(\mathbf{q},\mathbf{p})\in\mathcal{X}$ we require $K_H((\mathbf{q},\mathbf{p}),A)>0$. For S volume preserving, it suffices that

$$\forall\,\mathbf{q}'\in\mathcal{Q},\ \exists\,\tilde{\mathbf{p}}\in\mathcal{P},\quad \text{such that}$$
$$S(\mathbf{q},\tilde{\mathbf{p}})=(\mathbf{q}',\mathbf{p}')\ \text{for some}\ \mathbf{p}'. \tag{12}$$

Then for $A\subseteq B$ measurable, the set $P^1_{\mathbf{q},A}=\{\mathbf{p}:S(\mathbf{q},\mathbf{p})\in A\}$ of momenta that take $\mathbf{q}$ to A in one step is also measurable (i.e., $\pi(P^1_{\mathbf{q},\mathbf{A}})>0$), and therefore,

$$K_H((\mathbf{q},\mathbf{p}),A)\geqslant\int_{P^1_{\mathbf{q},A}} f(\tilde{\mathbf{p}})\alpha((\mathbf{q},\tilde{\mathbf{p}}),S(\mathbf{q},\tilde{\mathbf{p}}))d\tilde{\mathbf{p}}>0, \tag{13}$$

since $f(\mathbf{p}')$ and $\alpha((\mathbf{q},\mathbf{p}),(\mathbf{q}',\mathbf{p}'))$ are strictly positive for $\mathcal{H}(\mathbf{q}',\mathbf{p}')<\infty$. To see that Eq. (12) holds for the leap-frog integrator (2), note that for any $\tilde{\mathbf{q}}\in\mathcal{Q}$ we have $\tilde{\mathbf{p}}_i=m_i(\tilde{\mathbf{q}}_i-\mathbf{q}_i)/\Delta t+(\partial/\partial\mathbf{q}_i)U(\mathbf{q})(\Delta t/2)$. To see that Eq. (12) holds for Nosé–Poincaré, note that for any $\mathbf{q}$, $\tilde{\mathbf{q}}$, and any s, p_s we have $\tilde{\mathbf{p}}_i=(m_i(\tilde{\mathbf{q}}_i-\mathbf{q}_i)/\Delta t+(\partial/\partial\mathbf{q}_i)U(\mathbf{q})(\Delta t/2))s(1+p_s\Delta t/4Q)^2$. To see that this argument remains true for $L>1$, recall that S is volume preserving and time reversible, so A measurable implies $S^{-L}(A)$ measurable implies $P^1_{\mathbf{q},S^{-L}(A)}$ measurable, and Eq. (13) holds with S replaced by S^L.

Therefore we have $K_H(\mathbf{x},A)>0$ for all $\mathbf{x}\in\mathcal{X}$ and $\phi(A)>0$, so HMC is (strongly) ϕ-irreducible, and therefore irreducible and ergodic. □

B. Langevin dynamics

For comparison, we include another common choice for stochastic dynamics, namely, Langevin dynamics. Langevin dynamics is described by the stochastic ordinary differential equation,

$$d\mathbf{q}=\mathbf{p}dt,$$

$$d\mathbf{p}=-\gamma\mathbf{p}dt-\nabla U(\mathbf{q})+\sigma dW,$$

where W is standard p-dimensional Brownian motion, and U is the potential energy as before. We use the popular BBK integrator,[48]

$$\mathbf{p}_i(t+\Delta t/2)=\left(1-\frac{\gamma\Delta t}{2}\right)\mathbf{p}_i(t)+\frac{\Delta t}{2}\left(-\frac{\partial U}{\partial\mathbf{q}_i}+\frac{\sigma}{\sqrt{\Delta t}}Z(t)\right),$$

$$\mathbf{q}_i(t+\Delta t)=\mathbf{q}_i(t)+\Delta t\mathbf{p}_i\left(t+\frac{\Delta t}{2}\right),$$

$$\mathbf{p}_i(t+\Delta t)=\frac{\mathbf{p}_i\left(t+\frac{\Delta t}{2}\right)+\frac{\Delta t}{2}\left(-\frac{\partial U}{\partial\mathbf{q}_i}+\frac{\sigma}{\sqrt{\Delta t}}Z(t+\Delta t)\right)}{1+\frac{\gamma\Delta t}{2}},$$

where $Z(t)$ is a vector of standard normal random variables.

Because of the random motion introduced by the Brownian motion, Langevin dynamics is irreducible, and has been shown to be ergodic under certain conditions on $U(\mathbf{q})$ and for specific integrators.[49] However, those conditions are not satisfied by standard molecular mechanics forcefields and in-

tegrators, and it remains to be seen if ergodicity can be established for these systems. As such the Langevin dynamics results in Sec. VII are provided only for illustration. Note that when HMC is applied to Langevin dynamics ($L=1$), it yields an algorithm similar to the Metropolis-corrected Langevin diffusion algorithm[50] which corrects for the numerical error introduced by discretizing Langevin diffusion. However, it is unclear if this remains measure-preserving using the BBK integrator.

VII. EXAMPLES

The practical impact of the failures of invariance and ergodicity described in the previous sections can be illustrated on simple examples, where the effect on the entire ensemble may be visualized directly.

A. Harmonic oscillators and Gaussian mixtures

We first consider two model Hamiltonian systems. The first has target Boltzmann distribution given by a bivariate standard normal (Gaussian) distribution,

$$\pi_1(\mathbf{q}) = \frac{1}{2\pi\sigma^2}\exp\left\{-\frac{1}{2\sigma^2}\|\mathbf{q}\|^2\right\},$$

and the second given by a mixture of bivariate normals centered at (0,0) and (8,8), respectively,

$$\pi_2(\mathbf{q}) = \frac{\rho}{2\pi\sigma^2}\exp\left\{-\frac{1}{2\sigma^2}\|\mathbf{q}\|^2\right\} + \frac{(1-\rho)}{2\pi\sigma^2}\exp\left\{-\frac{1}{2\sigma^2}\|\mathbf{q}-8\|^2\right\}.$$

In the examples below we use $\sigma^2=1$ and $\rho=\frac{1}{2}$. Taking $k_BT=\sigma^2$, the potential energy of π_1 is given by $U(\mathbf{q})=-\log(\pi_1(\mathbf{q}))=\log 2\pi+\frac{1}{2}\Sigma_{i=1}^2 q_i^2$. Combining this with a kinetic term $K(\mathbf{p})=\frac{1}{2}\Sigma_{i=1}^2 p_i^2$ (with masses $m_1=m_2=1$) yields the Hamiltonian,

$$\mathcal{H}_1(\mathbf{q},\mathbf{p}) = U(\mathbf{q}) + K(\mathbf{p}) = \log 2\pi + \frac{1}{2}\sum_{i=1}^{2} q_i^2 + \frac{1}{2}\sum_{i=1}^{2} p_i^2, \tag{14}$$

and the resulting Hamiltonian system,

$$\dot{\mathbf{q}}_i = \frac{\partial\mathcal{H}_1}{\partial\mathbf{p}_i} = \mathbf{p}_i, \quad \dot{\mathbf{p}}_i = -\frac{\partial\mathcal{H}_1}{\partial\mathbf{q}_i} = -\mathbf{q}_i,$$

is easily recognized as simple harmonic motion in the plane, with solution

$$\mathbf{q}_i = A_i\cos t + B_i\sin t, \tag{15}$$

obtained by writing the system as a linear second order differential equation $\ddot{\mathbf{q}}_i=-\mathbf{q}_i$, where $\mathbf{q}_0=(A_1,A_2)$ and $\mathbf{p}_0=(B_1,B_2)$ are the initial position and momentum, respectively. Although Eq. (15) is the unique solution for (14) with initial conditions $(\mathbf{q}_0,\mathbf{p}_0)$, this solution trajectory does not reach all points of equal energy from a single initial condition, but instead traverses a set of points of equal energy along the curves $\mathbf{q}_i=A_i\cos t+B_i\sin t$. Thus, the Hamiltonian dynamics fail to be ergodic even under the microcanonical ensemble.

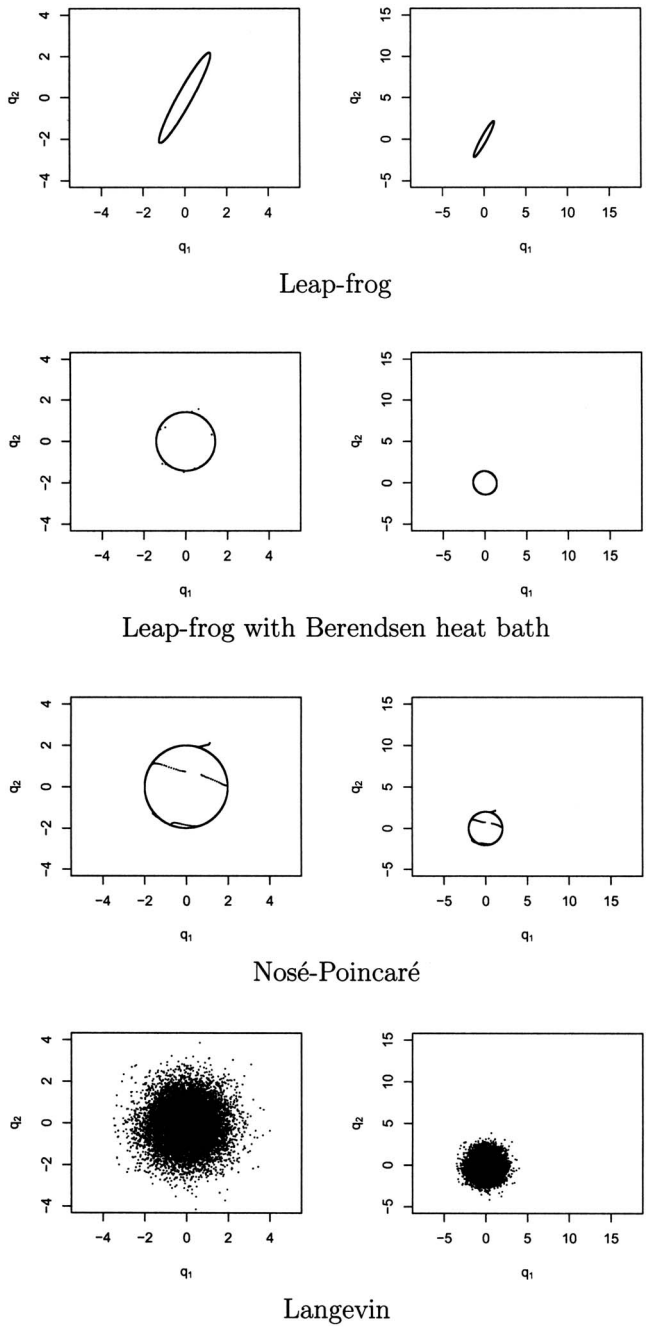

FIG. 1. Comparison of four dynamics simulation algorithms for the target distributions π_1 (left column) and π_2 (right column) defined in text. Algorithms are (top to bottom): microcanonical dynamics using leap-frog integrator; canonical dynamics using Berendsen heat bath; canonical dynamics using Nosé–Poincaré integrator; and canonical Langevin dynamics.

Similarly, the Hamiltonian for π_2 is of the form

$$\mathcal{H}_2(\mathbf{q},\mathbf{p}) = \log(e^{-(1/2)\|\mathbf{q}\|^2} + e^{-(1/2)\|\mathbf{q}-8\|^2}) + \tfrac{1}{2}\|\mathbf{p}\|^2 - \log(4\pi).$$

Dynamical simulation of these Hamiltonian systems can therefore be applied to generate the corresponding Boltzmann ensembles π_1 and π_2.

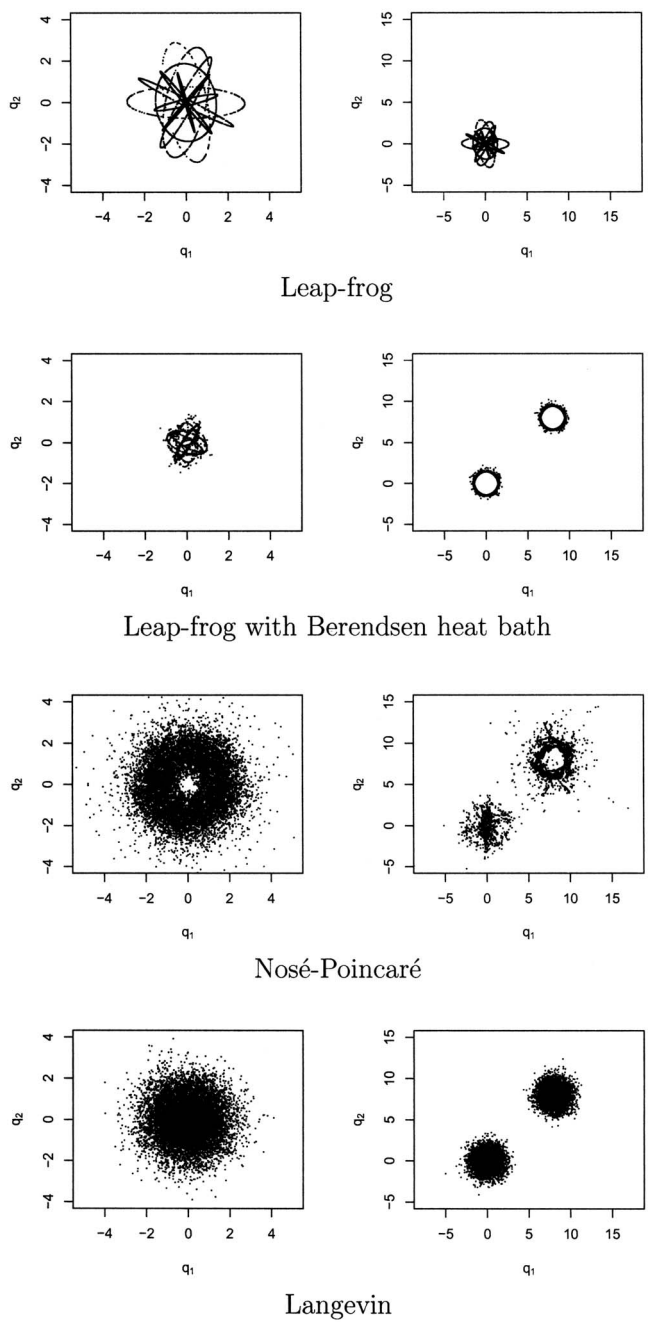

FIG. 2. Replica-exchange dynamics using each of the four dynamics algorithms, for simulating π_1 (left) and π_2 (right). Each REMD involves ten replicas of the corresponding dynamics.

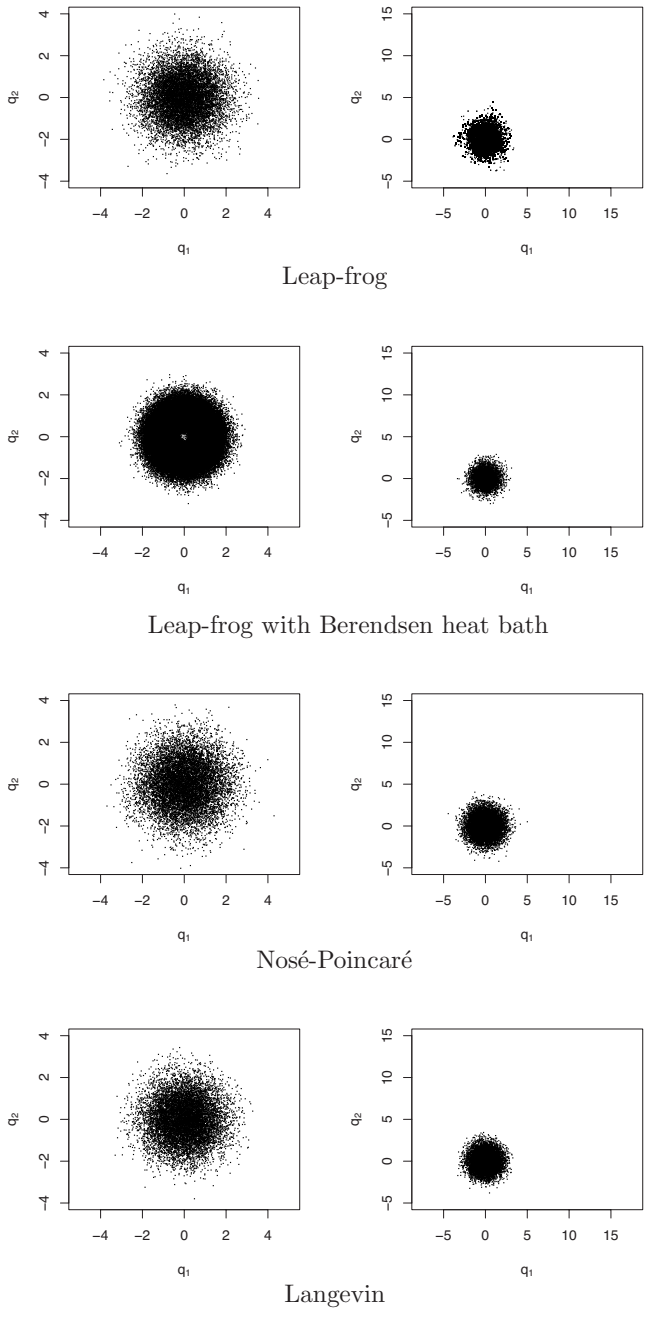

FIG. 3. The four dynamics algorithms of Fig. 1, augmented with the hybrid Monte Carlo correction described in text.

1. Numerical results

To demonstrate the practical impact of the theoretical results of Sec. V C on commonly used biomolecular simulation protocols, we compare several of the dynamics analyzed in previous sections for simulating the Boltzmann ensembles π_1 and π_2: microcanonical dynamics with a leap-frog integrator, canonical dynamics based on leap-frog with Berendsen heat bath, Nosé-Poincaré, and stochastic Langevin dynamics. (Nosé–Hoover was not included because, based on the lack of measure-invariance as discussed in Sec. V, we consider it to be superseded by NP. Both NH and NP fail to be ergodic as shown in Sec. V, but NP with its symplectic integrator is measure invariant, and can thus be made ergodic by using the stochastic HMC correction—see Sec. VI A.)

Leap-frog (with or without a Berendsen heat bath) and Langevin dynamics used a step size of 0.1 s, and Nosé–Poincaré used a 0.01 s step size. Simulations without hybrid Monte Carlo or replica exchange were run for 100 000 steps, or 1000 s. Hybrid Monte Carlo proposal trajectories utilized $L=50$ steps of the corresponding numerical integrator (leap-frog, leap-frog with Berendsen with $\tau_T=10$, BBK, or the Nosé–Poincaré integrator (Appendix A 2). Step sizes and L were chosen to achieve a HMC acceptance rate between 20% and 60%. REMD utilized 10 parallel MD simulations, attempted swaps every 100 steps, and ran for 1000 s. Replica

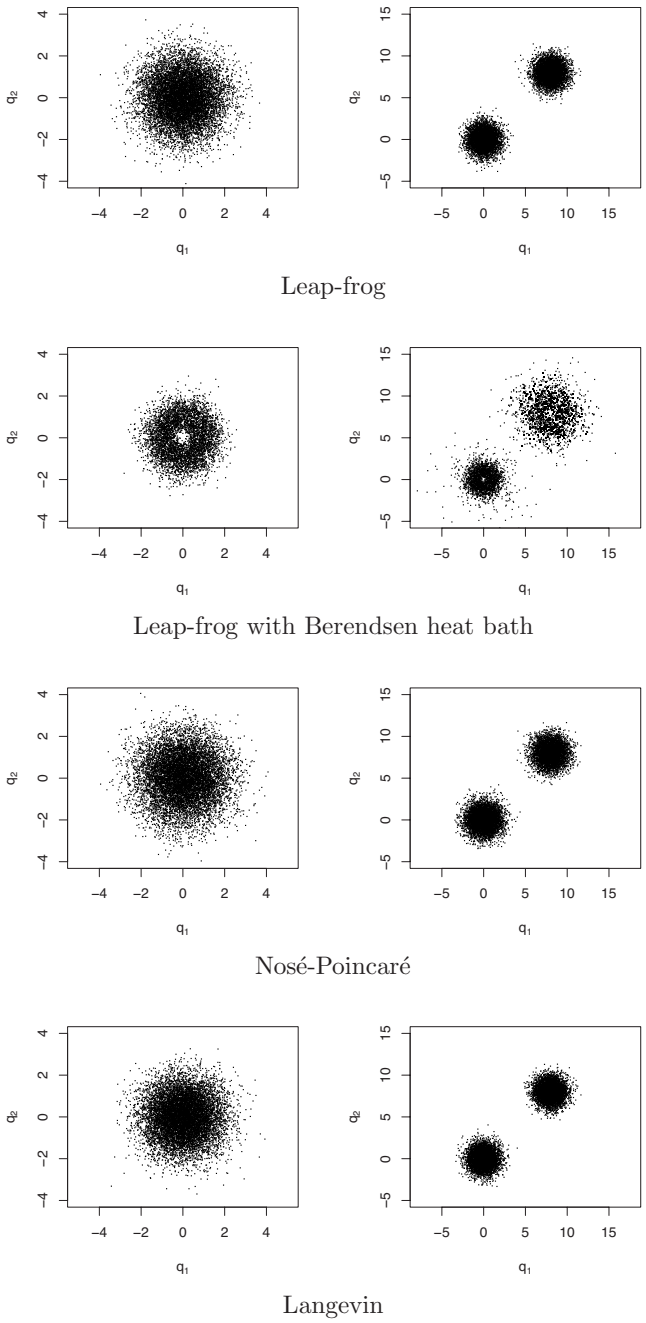

FIG. 4. Replica-exchange simulations using the four respective dynamics algorithms, each with the hybrid Monte Carlo correction. The microcanonical and Langevin algorithms thus become parallel tempering HMC and parallel tempering Langevin dynamics, respectively, both of which are measure invariant and ergodic.

exchange with hybrid Monte Carlo followed each 50 step trajectory with a Metropolis acceptance, before proposing a temperature swap.

The results of these simulations are shown in Figs. 1–4. In each figure, simulations of π_1 are shown in the left column, and π_2 in the right. Figure 1 compares microcanonical MD and canonical MD via a Berendsen heat bath, Nosé–Poincaré, and Langevin dynamics, for both target distributions. It is clearly seen that the microcanonical, Berendsen, and Nosé–Poincaré dynamics are not ergodic. The Nosé–Poincaré shows clear signs of not being able to reach the low-energy region near the origin, as indicated in Sec. V C as a potential consequence of Theorem 5.5. Langevin dynamics (without the HMC correction) appears to generate the target ensemble π_1, but fails to cross the energy barrier in π_2.

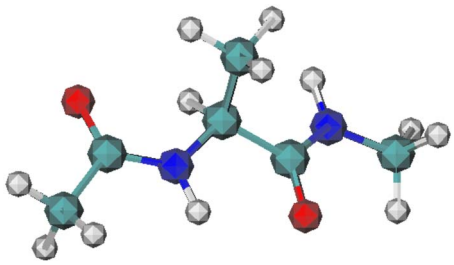

FIG. 5. (Color online) Molecular structure of alanine dipeptide.

Figure 2 compares REMD simulations, each performed using the respective isothermal dynamics algorithm for its (10) individual replicas. Again microcanonical dynamics generates constant-$\mathcal{H}$ trajectories dependent on the initial coordinates; since each replica has distinct random initial coordinates, many additional trajectories are observed, but the simulation clearly still fails to be ergodic. Similarly, the Berendsen thermostat again fails to generate the correct ensemble. Nosé–Poincaré appears to remain reducible, restricted to orbits based on initial coordinates. Langevin dynamics is now able to cross the energy barrier in π_2, and appears to generate both ensembles correctly.

Figure 3 repeats the experiments of Fig. 1 (without replica-exchange), but utilizing the hybrid Monte Carlo correction described in Sec. VI. The microcanonical dynamics now becomes standard Hybrid Monte Carlo[42] and is ergodic as proven in Sec. VI, thus will generate the correct π_1 ensemble. However, it fails to cross the energy barrier of π_2 in the absence of replica exchange. (Although it is ergodic and will eventually cross with probability one, this may take a long time.) The Berendsen thermostat still shows significant artifacts arising from it's failure to be measure-preserving. Nosé–Poincaré actually crosses the barrier of π_2, but not sufficiently easily to equilibrate between the two energy wells without replica exchange. Langevin dynamics also fails to cross the energy barrier of π_2 in the absence of replica exchange.

Finally, Fig. 4 shows the results of using the HMC correction in combination with replica exchange. In this case all of the algorithms except the Berendsen thermostat are measure-preserving and ergodic, and able to cross the energy barrier, so generate the correct ensembles for both π_1 and π_2. Note that in these cases, there is no distinction between "replica-exchange" using the HMC correction, and the original parallel tempering algorithm;[2] the underlying Markov chains just happen to be being generated by hybrid Monte Carlo.[42,45] The Berendsen thermostat, which is not measure-preserving, still clearly fails to converge to the proper ensembles as expected.

B. Alanine dipeptide

To demonstrate the implications for a molecular system under a standard forcefield, we simulated the small Alanine dipeptide (see Fig. 5) under REMD using the Berendsen

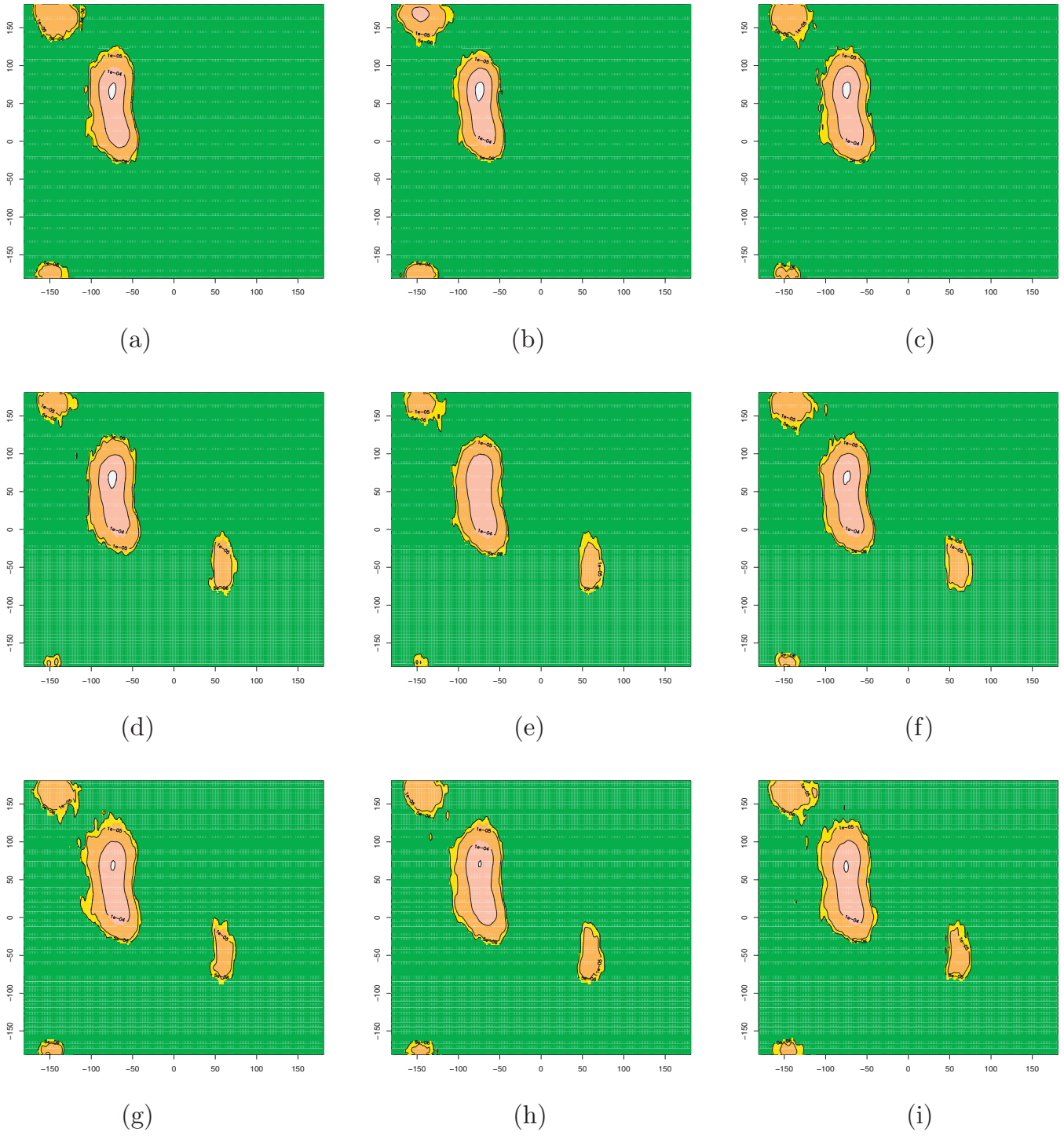

FIG. 6. (Color) Heatmap plots with an overlayed contour plot of the Ramachandran plots generated by the 273 K replica of the REMD simulations of Alanine dipeptide with Berendsen coupling [(a)–(c)] vs Hybrid Monte Carlo [(d)–(f)]. Also shown for comparison are Langevin dynamics [(g)–(i)]. Simulations were started from the three major energy well regions of (ϕ,ψ) space [$(-75,40)$ for (a), (e), and (g), $(-150,160)$ for (b), (d), and (h), $(60,-50)$ for (c), (f), and (i)], and run to equilibrium.

thermostat as commonly done in practice for peptide simulations,[1,6,25–28] and compared the results to those obtained using parallel tempering with hybrid Monte Carlo, which we have shown guarantees invariance and ergodicity. Results for Langevin dynamics are also shown for comparison; implementations of NH and NP are not available in the AMBER and NAMD packages used. Alanine dipeptide has been extensively studied computationally and experimentally; we choose it here because the molecule has only two internal dihedral angles, making it possible to ensure adequate sampling quickly, and to easily visualize the generated ensemble. Each simulation was run without solvent under the AMBER94 forcefield as implemented in the NAMD suite of programs,[31] with 1 fs time step and 10 Å cutoff, at a target temperature T_0 of 273 K.

In each case, three Berendsen-coupling REMD, three HMC parallel tempering, and three Langevin dynamics parallel tempering simulations were run, each using ten replicas

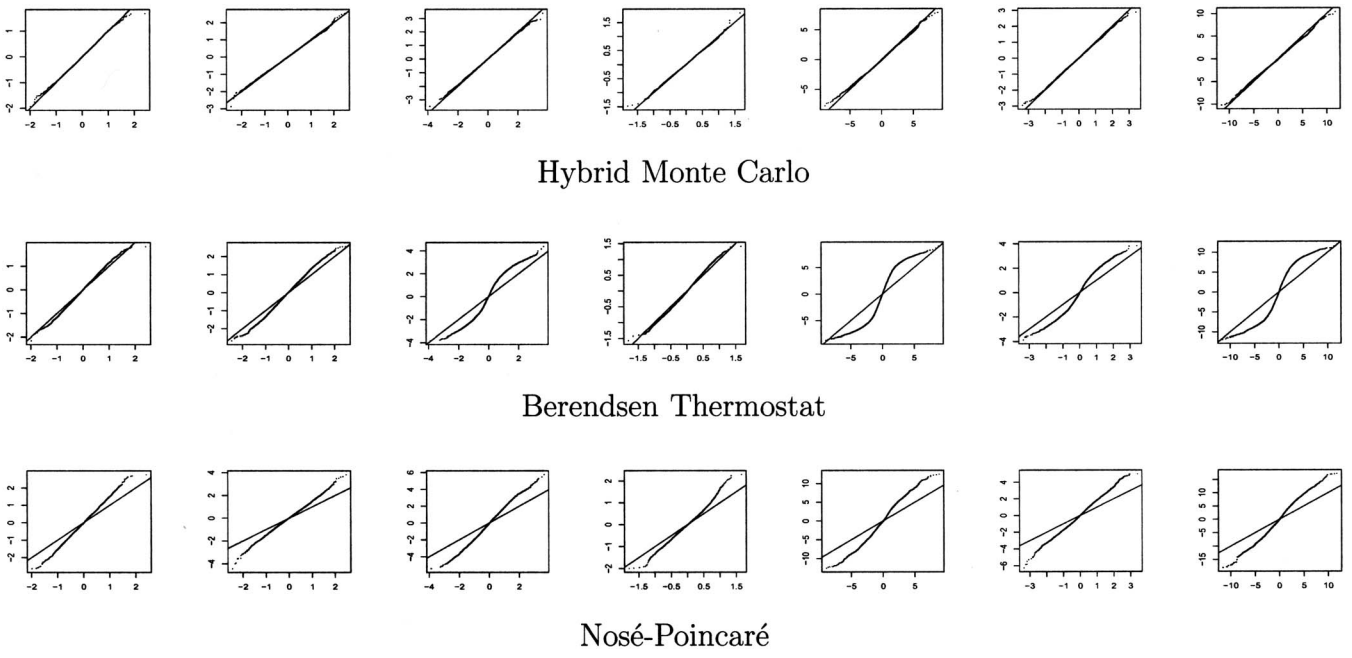

FIG. 7. Normal quantile-quantile plots for the marginal distributions of dimensions one through seven, calculated from the ensembles generated by the hybrid Monte Carlo (first row), Berendsen (second row), and Nosé–Poincaré (third row) algorithms for the high-dimensional random-covariance target ensemble described in the text. Deviations from the diagonal represent departures from the true ensemble, with the "S" shape indicating heavy tails: regions near the energy minimum are significantly undersampled by the non-HMC algorithms.

with temperatures distributed exponentially between 273 and 2000 K, and swaps between neighboring temperatures attempted every 100 steps. For all three algorithms, the three simulations were initialized to three distinct ϕ/ψ conformations, representing regions of favorable energy determined by trial simulations and confirmed in previous studies in the literature: $(\phi,\psi)\in\{(-75,40),(-150,160),(60,-50)\}$. Total running time was 2 ns per replica, well beyond that needed for equilibration and production phases; convergence was established using parallel simulation convergence diagnostics as described previously.[6]

The resulting ensembles generated at T_0 (273 K) are shown in Fig. 6. The non-measure-preserving Berendsen thermostat has clearly altered the target Boltzmann ensemble, to the extent that an entire energy well ($\phi>0$) is not preserved. Note that the Berendsen MD leaves that region even when initialized there and never returns, indicating that with REMD it is not a mixing problem. (In the absence of replica exchange, Langevin dynamics is unable to cross the barrier between energy wells even in this small system, sampling the $\phi>0$ region only when initialized there; plots not shown.) This example demonstrates that for molecular systems under standard forcefields, the failure of the commonly used Berendsen thermostat to be measure-preserving can have a significant impact on the ensemble simulated. Such effects clearly compromise attempts to validate and refine forcefields based on calculation of experimental quantities.

C. High-dimensional systems and irregular energy landscapes

It is often suggested that ergodicity problems such as those identified here arise only in small systems with low or weakly coupled degrees of freedom. However, our theorems of Sec. V hold for systems of *any* size. Thus, the belief that ergodicity failures do not persist in larger systems most likely simply reflects the difficulty of accurately observing complex high-dimensional ensembles. This confusion further emphasizes the importance of establishing formal proofs of algorithm properties, since empirical observation may fail to identify non-ergodic behavior in complex high-dimensional systems.

To demonstrate the persistence of these failures in higher dimensions and under more complex energy landscapes, we extended our simulation experiments to two additional target ensembles. These are (a) a 50-dimensional normal distribution $N(0,\Sigma)$ with random positive-definite covariance matrix Σ generated by $\Sigma=M^TM$, with M a 50×50 matrix of independent $N(0,1)$ random variates, generating a highly coupled and irregular energy landscape;[51] and (b) a two-component normal mixture in 50 dimensions, also highly coupled due to two distinct significant energy wells. For each target ensemble we performed REMD simulations using HMC, Berendsen, and Nosé–Poincaré as before; Langevin results were identical to HMC and are omitted for space. Although quantitative summarization and comparison of high-dimensional ensembles is difficult in general, the target ensembles here are chosen to enable this. In particular, the *marginal* distributions of ensemble (a) are all known (normal) and the samples can be evaluated for their ability to generate the correct marginals. Figure 7 shows normal quantile-quantile plots for the marginal distributions for the first seven degrees of freedom. Deviations from the diagonal represent departures from the correct distribution; the "S" shape indicates that the ensembles generated by the Berendsen and NP algorithms have insufficient samples near the mode (energy minimum) and too many farther away. This indicates the same

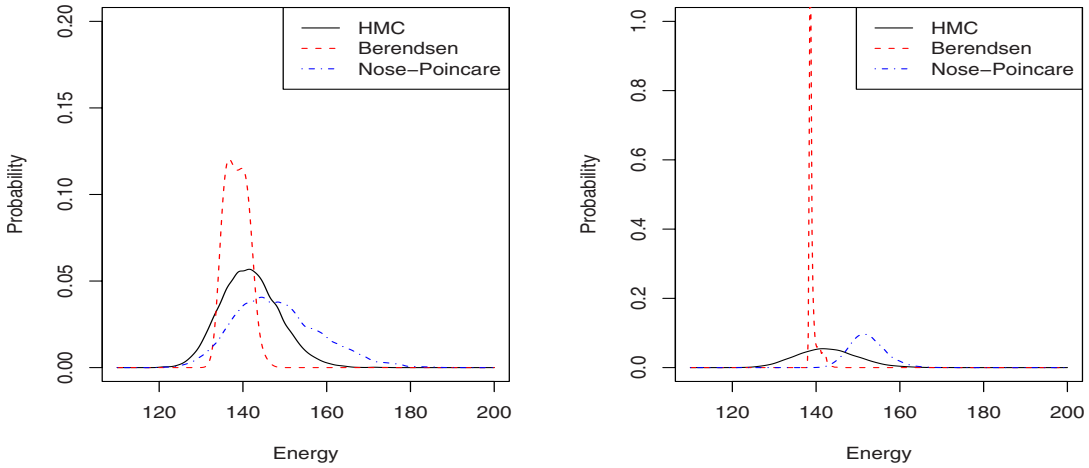

FIG. 8. (Color online) Energy histograms generated by Berendsen, Nosé-Poincaré, and hybrid Monte Carlo algorithms for two high-dimensional target ensembles: (a) 50-dimensional normal distribution with random covariance matrix, yielding highly irregular coupling, and (b) mixture of two 50-dimensional normals. These energy profiles indicate that the ensembles generated by Berendsen and NP deviate significantly from the correct ensemble generated by HMC.

sort of behavior shown in the two-dimensional case of Fig. 2, which is easier to visualize in 2D but as shown by the q-q plots still persists in high dimensions as well. For further comparison, Fig. 8 shows the energy histograms for the ensembles generated by the three algorithms. Again it is clear that the ensembles generated by the Berendsen and Nosé–Poincaré dynamics differ significantly from the correct ensemble generated by HMC.

VIII. DISCUSSION

A critical step in improving existing macromolecular forcefields is the comparison of simulated quantities to experimental measurements.[6,25,27] To make such comparisons quantitatively, the simulated quantities must accurately reflect the ensemble induced by the associated forcefield.[6] Here we have demonstrated that this is not the case for the implementations of replica-exchange molecular dynamics currently in common use for biomolecular simulation. Failures of isothermal molecular dynamics to yield correct ensembles and ergodic averages, either through failure to preserve measure or failure to be ergodic, persist when these algorithms are used as constant-temperature components of replica exchange. We have made explicit the theoretical shortcomings of commonly used algorithms, and demonstrated that these failures can have significant practical impact on even small systems. Our results demonstrate the importance of formal analysis of new simulation methods, where empirical studies may fail to show such defects simply due to the difficulties in evaluating correctness of high-dimensional ensembles.

Fortunately these failures come entirely from the use of deterministic dynamics, and stochastic versions are available which correct these theoretical and practical shortcomings. In deterministic dynamics simulations ergodicity must be *assumed*, and as we have shown this assumption is often incorrect; in contrast, for stochastic dynamics ergodicity can generally be guaranteed by basic theorems of stochastic processes. Since real macromolecules in solvent behave stochastically anyway, there appears to be little advantage to using purely deterministic dynamics methods. Arguments that stochastic thermostats disrupt the ability to simulate dynamic properties such as diffusion coefficients are common (see, e.g., Ref. 16, and most of the isothermal dynamics papers cited in Sec. V), but are in our view overwhelmed by the potential for failures in ergodicity. It is worth emphasizing that if the system is not ergodic, dynamic properties computed can not be assumed accurate in any case. Moreover, the use of replica-exchange dynamics to enable crossing of energy barriers already fundamentally disrupts the dynamics of the T_0 system by configuration swapping. Thus, we see little advantage to using deterministic replica-exchange molecular dynamics, over stochastic versions. In the latter case, REMD reduces to the original parallel tempering algorithm from which it was adapted.

APPENDIX A: INTEGRATORS FOR ISOTHERMAL DYNAMICS

1. Nosé–Hoover integrators

Winkler *et al.*[36] modified a time-reversible integrator developed by Toxvaerd[52] for Nosé–Hoover dynamics,

$$\mathbf{q}_i(t+\Delta t) = \mathbf{q}_i(t) + \frac{\mathbf{p}_i(t)}{m_i}\Delta t + \left[\frac{\partial}{\partial \mathbf{q}_i}U(\mathbf{q}(t)) - \zeta(t)\mathbf{p}_i(t)\right]\frac{\Delta t^2}{2m_i},$$

$$\mathbf{p}_i\left(t+\tfrac{1}{2}\Delta t\right) = \mathbf{p}_i(t) + \left[\frac{\partial}{\partial \mathbf{q}_i}U(\mathbf{q}(t)) - \zeta(t)\mathbf{p}_i(t)\right]\frac{\Delta t}{2},$$

$$\zeta(t+\Delta t) = \zeta(t) + \left[\sum_{i=1}^{N_f} m_i\|\mathbf{p}_i\|^2\left(t+\frac{1}{2}\Delta t\right) - gkT\right]\frac{\Delta t}{Q},$$

$$\mathbf{p}_i(t+\Delta t) = \left(\mathbf{p}_i\left(t+\tfrac{1}{2}\Delta t\right) + \left[\frac{\partial}{\partial \mathbf{q}_i}U(\mathbf{q}(t+\Delta t))\right]\frac{\Delta t}{2}\right) \Bigg/ \left(1+\zeta(t+\Delta t)\frac{\Delta t}{2}\right).$$

However, considering the phase space over the variables $(\mathbf{q},\mathbf{p},\zeta)$, we can see that the mapping is not volume preserving or symplectic. Define

$$R_1: \quad (\mathbf{q},\mathbf{p},\zeta) \mapsto (\mathbf{q}',\mathbf{p}',\zeta') = \left(\mathbf{q}+\frac{\mathbf{p}}{m}\Delta t + (F(\mathbf{q})-\zeta\mathbf{p})\frac{\Delta t}{2m}, \mathbf{p} + (F(\mathbf{q})-\zeta\mathbf{p})\frac{\Delta t}{2}, \zeta\right),$$

$$R_2: \quad (\mathbf{q}',\mathbf{p}',\zeta') \mapsto (\mathbf{q}'',\mathbf{p}'',\zeta'') = \left(\mathbf{q}',\mathbf{p}',\zeta+\left[\sum m_i(\mathbf{p}_i')^2 - gkT\right]\frac{\Delta t}{2}\right),$$

$$R_3: \quad (\mathbf{q}'',\mathbf{p}'',\zeta'') \mapsto (\mathbf{q}''',\mathbf{p}''',\zeta''') = \left(\mathbf{q}'', \left(\mathbf{p}''+F(\mathbf{q}'')\frac{\Delta t}{2}\right) \Bigg/ \left(1+\zeta''\frac{\Delta t}{2}\right), \zeta''\right).$$

Then the Jacobian of the composition map $S(\mathbf{q},\mathbf{p},\zeta)=R_3\circ R_2\circ R_1$ is

$$J_S = J_{R_3}J_{R_2}J_{R_1} = \begin{vmatrix} 1 & 0 & 0 \\ \frac{F'(\mathbf{q})}{2+\zeta\Delta t} & \frac{2}{2+\zeta\Delta t} & \frac{-2\mathbf{p}-F'(\mathbf{q})\Delta t}{(2+\zeta\Delta t)^2}\frac{\Delta t}{2} \\ 0 & 0 & 1 \end{vmatrix} \cdot \begin{vmatrix} 1 & 0 & 0 \\ 0 & 1 & 0 \\ 0 & \frac{m\Delta t}{Q}f(\mathbf{p}) & 1 \end{vmatrix} \cdot \begin{vmatrix} 1+F'(\mathbf{q})\frac{\Delta t^2}{2m} & \frac{\Delta t}{m}-\zeta\frac{\Delta t^2}{2m} & -\frac{\mathbf{p}\Delta t}{2m} \\ F'(\mathbf{q})\frac{\Delta t}{2} & 1-\zeta\frac{\Delta t}{2}, & -\frac{\mathbf{p}\Delta t}{2} \\ 0 & 0 & 1 \end{vmatrix} = \frac{2-\zeta\Delta t}{2+\zeta\Delta t},$$

so $J_S<1$ for $\Delta t>0$. Winkler *et al.*[36] also introduced an alternative method, but it is not phase-space volume preserving for systems with many degrees of freedom such as polypeptides.

2. Nosé–Poincaré integrators

Nosé[39] gives an explicit, time-reversible, symplectic integrator for the Nosé–Poincaré dynamics,

$$s_i\left(t+\tfrac{1}{2}\Delta t\right) = s_i(t)\left(1+\frac{p_s(t)}{2Q}\frac{\Delta t}{2}\right)^2,$$

$$p_s^* = \frac{p_s(t)}{1+\frac{p_s(t)}{2Q}\frac{\Delta t}{2}},$$

$$\mathbf{p}_i\left(t+\frac{\Delta t}{2}\right) = \mathbf{p}_i(t) - s\left(t+\frac{\Delta t}{2}\right)\frac{\partial}{\partial \mathbf{q}_i}U(\mathbf{q}(t))\frac{\Delta t}{2},$$

$$\mathbf{q}_i(t+\Delta t) = \mathbf{q}_i(t) + \frac{\mathbf{p}_i\left(t+\frac{\Delta t}{2}\right)}{m_i s\left(t+\frac{\Delta t}{2}\right)}\Delta t,$$

$$\mathbf{p}_i(t+\Delta t) = \mathbf{p}_i\left(t+\frac{\Delta t}{2}\right) - s\left(t+\frac{\Delta t}{2}\right)\frac{\partial}{\partial \mathbf{q}_i}U(\mathbf{q}(t+\Delta t))\frac{\Delta t}{2},$$

$$p_s^{**} = p_s^* + \left[\sum_i \frac{1}{2m_i}\left(\frac{\mathbf{p}_i(t+\Delta t)}{s\left(t+\frac{\Delta t}{2}\right)}\right)^2 - \tfrac{1}{2}(U(\mathbf{q}(t)) + U(\mathbf{q}(t+\Delta t))) - gkT\ln s\left(t+\frac{\Delta t}{2}\right) + H_0 - gkT\right]\Delta t,$$

$$s(t+\Delta t) = s\left(t+\frac{\Delta t}{2}\right)\left(1+\frac{p_s^{**}}{2Q}\frac{\Delta t}{2}\right)^2,$$

$$p_s(t+\Delta t) = \frac{p_s^{**}}{1+\frac{p_s(t)}{2Q}\frac{\Delta t}{2}}.$$

We can see that this integrator preserves phase-space volume by writing the mappings,

$$R_1:(\mathbf{q},\mathbf{p},s,p_s) \mapsto \left(\mathbf{q},\mathbf{p},s\left(1+\frac{p_s}{2Q}\frac{\Delta t}{2}\right)^2, \frac{p_s}{1+\frac{p_s}{2Q}\frac{\Delta t}{2}}\right),$$

$$R_2:(\mathbf{q},\mathbf{p},s,p_s) \mapsto \left(\mathbf{q},\mathbf{p}-sF(\mathbf{q})\frac{\Delta t}{2},s,p_s\right),$$

$$R_3:(\mathbf{q},\mathbf{p},s,p_s) \mapsto \left(\mathbf{q}+\frac{\mathbf{p}\Delta t}{ms},\mathbf{p},s,p_s\right),$$

$$R_4:(\mathbf{q},\mathbf{p},s,p_s) \mapsto \left(\mathbf{q},\mathbf{p}-sF(\mathbf{q})\frac{\Delta t}{2},s,p_s+\left[\frac{|\mathbf{p}|^2}{2ms^2} - \tfrac{1}{2}(U(\mathbf{q})+U(\mathbf{q}')) - gkT\ln s + H_0 - gkT\right]\Delta t\right),$$

and noting that the integration mapping J_S is a composition $J_S = J_{R_1} \circ J_{R_4} \circ J_{R_3} \circ J_{R_2} \circ J_{R_1}$, and verifying that $|J_{R_1}| = |J_{R_2}| = |J_{R_3}| = |J_{R_4}| = 1$,

$$|J_S| = |J_{R_1}| \cdot |J_{R_4}| \cdot |J_{R_5}| \cdot |J_{R_2}| \cdot |J_{R_1}| = \begin{vmatrix} 1 & 0 & 0 & 0 \\ 0 & 1 & 0 & 0 \\ 0 & 0 & \left(1 + \frac{p_s \Delta t}{4Q}\right)^2 & 2s\left(1 + \frac{p_s}{2Q}\frac{\Delta t}{2}\right)\frac{\Delta t}{4Q} \\ 0 & 0 & 0 & 1 \Big/ \left(1 + \frac{p_s \Delta t}{4Q}\right)^2 \end{vmatrix} \cdot \begin{vmatrix} 1 & 0 & 0 & 0 \\ sF'(\mathbf{q})\frac{\Delta t}{2} & 1 & -F(\mathbf{q})\frac{\Delta t}{2} & 0 \\ 0 & 0 & 1 & 0 \\ 0 & 0 & 0 & 1 \end{vmatrix}$$

$$\cdot \begin{vmatrix} 1 & \frac{\Delta t}{ms} & -\frac{p\Delta t}{ms^2} & 0 \\ 0 & 1 & 0 & 0 \\ 0 & 0 & 1 & 0 \\ 0 & 0 & 0 & 1 \end{vmatrix} \cdot \begin{vmatrix} 1 & 0 & 0 & 0 \\ -sF'(\mathbf{q})\frac{\Delta t}{2} & 1 & -F'(\mathbf{q})\frac{\Delta t}{2} & 0 \\ 0 & 0 & 1 & 0 \\ F(\mathbf{q}) + F(\mathbf{q}^*) & \frac{1}{2ms}G(\mathbf{q}) & -\frac{|\mathbf{p}|^2}{ms^3} - \frac{gkT}{s} & 1 \end{vmatrix}$$

$$\cdot \begin{vmatrix} 1 & 0 & 0 & 0 \\ 0 & 1 & 0 & 0 \\ 0 & 0 & \left(1 + \frac{p_s \Delta t}{4Q}\right)^2 & 2s\left(1 + \frac{p_s}{2Q}\frac{\Delta t}{2}\right)\frac{\Delta t}{4Q} \\ 0 & 0 & 0 & 1 \Big/ \left(1 + \frac{p_s \Delta t}{4Q}\right)^2 \end{vmatrix} = 1.$$

[1] Y. Sugita and Y. Okamoto, Chem. Phys. Lett. **314**, 141 (1999).
[2] C. J. Geyer, Markov chain Monte Carlo maximum likelihood, in Computing Science and Statistics: Proceedings of the 23rd Symposium on Interface, 1991, pp. 156–163.
[3] P. H. Nguyen, Y. Mu, and G. Stock, Proteins: Struct., Funct., Genet. **60**, 485 (2005).
[4] M. M. Seibert, A. Patriksson, B. Hess, and D. van der Spoel, J. Mol. Biol. **354**, 173 (2005).
[5] W. Zhang, C. Wu, and Y. Duan, J. Chem. Phys. **123**, 154105 (2005).
[6] B. Cooke and S. C. Schmidler, "Statistical prediction and molecular dynamics simulation," Biophys. J. (in press).
[7] D. A. Beck, G. W. White, and V. Daggett, J. Struct. Biol. **157**, 514 (2007).
[8] X. Periole and A. E. Mark, J. Chem. Phys. **126**, 014903 (2007).
[9] A. E. Roitberg, A. Okur, and C. Simmerling, J. Phys. Chem. B **111**, 2415 (2007).
[10] N. Madras and Z. Zheng, Random Struct. Algorithms **1**, 66 (2003).
[11] D. Woodard, S. C. Schmidler, and M. Huber, "Conditions for rapid mixing of parallel and simulated tempering on multimodal distributions," Ann. Appl. Probab. (to be published).
[12] N. Bhatnagar and D. Randall, "Torpid mixing of simulated tempering on the Potts model," in Proceedings of the 15th ACM/SIAM Symposium on Discrete Algorithms (SODA), 2004, pp. 478–487.
[13] D. Woodard, S. C. Schmidler, and M. Huber, "Sufficient conditions for torpid mixing of parallel and simulated tempering on multimodal distributions," Electron. J. Probab. (submitted).
[14] M. P. Allen and D. J. Tildesley, *Computer Simulation of Liquids* (Oxford University Press, New York, 1987).
[15] D. J. Evans and G. P. Morriss, *Statistical Mechanics of Non-Equilibrium Liquids* (Academic, New York, 1990).
[16] D. Frenkel and B. Smit, *Understanding Molecular Simulation* (Academic, New York, 1996).
[17] A. R. Leach, *Molecular Modelling: Principles and Applications* (Addison Wesley Longman, New York, 1996).
[18] P. Billingsley, *Probability and Measure*, 3rd ed. (Wiley, New York, 1995).
[19] G. H. Choe, *Computational Ergodic Theory* (Springer-Verlag, Berlin, 2005).
[20] For ease of exposition we suppress formal statement of certain technical conditions; e.g., all sets and transformations considered are assumed to be π-measurable, and limits hold π-almost everywhere.
[21] N. Metropolis, A. W. Rosenbluth, M. N. Rosenbluth, A. H. Teller, and E. Teller, J. Chem. Phys. **21**, 1087 (1953).
[22] V. I. Arnold, *Mathematical Methods of Classical Mechanics* 2nd ed. (Springer-Verlag, Berlin, 1989).
[23] P. J. Channell and C. Scovel, Nonlinearity **3**, 231 (1990).
[24] H. J. C. Berendsen, J. P. M. Postma, W. F. van Gunsterenand, A. DiNola, and J. R. Haak, J. Chem. Phys. **81**, 3684 (1984).
[25] X. Daura, B. Juan, D. Seebach, W. F. van Gunsteren, and A. E. Mark, J. Mol. Biol. **280**, 925 (1998).
[26] X. Daura, K. Gademann, B. Jaun, D. Seebach, and W. F. van Gunsteren, Angew. Chem., Int. Ed. **38**, 236 (1999).
[27] A. E. Garcia and K. Y. Sanbonmatsu, Proc. Natl. Acad. Sci. U.S.A. **99**, 2782 (2002).
[28] L. J. Smith, X. Daura, and W. F. van Gunsteren, Proteins: Struct., Funct., Genet. **48**, 487 (2002).
[29] H. Nymeyer and A. E. Garcia, Proc. Natl. Acad. Sci. U.S.A. **100**, 13934 (2003).
[30] D. A. Pearlman *et al.*, Comput. Phys. Commun. **91**, 1 (1995).
[31] J. C. Phillips *et al.*, J. Comput. Chem. **26**, 1781 (2005).
[32] E. Lindahl, B. Hess, and D. van der Spoel, J. Mol. Model. **7**, 306 (2001).
[33] T. Morishita, J. Chem. Phys. **113**, 2976 (2000).
[34] S. Nosé, J. Chem. Phys. **81**, 511 (1984).
[35] W. G. Hoover, Phys. Rev. A **31**, 1695 (1985).
[36] R. G. Winkler, V. Kraus, and P. Reineker, J. Chem. Phys. **102**, 9018 (1995).
[37] G. J. Martyna, M. L. Klein, and M. Tuckerman, J. Chem. Phys. **97**, 2635 (1992).
[38] S. D. Bond, B. J. Leimkuhler, and B. B. Laird, J. Comput. Phys. **151**, 114 (1999).
[39] S. Nosé, J. Phys. Soc. Jpn. **70**, 75 (2001).
[40] B. B. Laird and B. J. Leimkuhler, Phys. Rev. E **68**, 016704 (2003).
[41] B. J. Leimkuhler and C. R. Sweet, J. Chem. Phys. **121**, 108 (2004).
[42] S. Duane, A. D. Kennedy, B. J. Pendleton, and D. Roweth, Phys. Lett. B

195, 216 (1987).
[43] R. W. Pastor, in *The Molecular Dynamics of Liquid Crystals*, edited by G. R. Luckhurst and C. A. Veracini (Kluwer Academic, Dordrecht, 1994), pp. 85–138.
[44] W. K. Hastings, Biometrika **57**, 97 (1970).
[45] R. M. Neal, "Probabilistic inference using Markov chain Monte Carlo methods," Technical Report No. CRG-TR-93-1, University of Toronto, 1993.
[46] J. S. Liu, *Monte Carlo Strategies in Scientific Computing* (Springer-Verlag, Berlin, 2001).
[47] S. P. Meyn and R. L. Tweedie, *Markov Chains and Stochastic Stability* (Springer-Verlag, Berlin, 1993).
[48] A. Brünger, C. Brooks III, and M. Karplus, Chem. Phys. Lett. **105**, 495 (1984).
[49] J. Mattingly, A. M. Stuart, and D. J. Higham, Stochastic Proc. Appl. **101**, 185 (2002).
[50] G. O. Roberts and R. L. Tweedie, Bernoulli **2**, 341 (1996).
[51] G. O. Roberts and J. S. Rosenthal "Examples of adaptive MCMC," J. Comp. Graph. Stat. (unpublished).
[52] S. Toxvaerd, Phys. Rev. E **47**, 343 (1993).